THE PENNSYLVANIA STATE UNIVERSITY
SCHREYER HONORS COLLEGE

DEPARTMENT OF ASTRONOMY & ASTROPHYSICS

A REANALYSIS TO EXTEND THE PLANETARY NEBULA LUMINOSITY FUNCTION INTO THE HUBBLE FLOW

OWEN CHASE
SPRING 2022

A thesis
submitted in partial fulfillment
of the requirements
for baccalaureate degrees
in Astronomy & Astrophysics and Statistics
with honors in Astronomy & Astrophysics

Reviewed and approved* by the following:

Robin Ciardullo
Professor of Astronomy & Astrophysics
Thesis Supervisor

Steinn Sigurdsson
Professor of Astronomy & Astrophysics
Honors Adviser

*Electronic approvals are on file in the Schreyer Honors College.

Abstract

The [O III] $\lambda 5007$ planetary nebula luminosity function (PNLF) is a well-established distance indicator for galaxies out to at least $\sim$10 Mpc. However, systematic discrepancies with other methods emerge at larger distances, and it reaches its effective limit at around 20 Mpc. Thus, the PNLF has recently fallen out of favor compared to methods like tip of the red giant branch (TRGB) and surface brightness fluctuations (SBF). In order to bring the PNLF into the modern era of precision cosmology and make it a competitive method for addressing the Hubble Tension, it is imperative to address the higher order sources of systematic error. A central issue with the PNLF is contamination from "overluminous" planetary nebulae (PNe). These overluminous objects tend to result in smaller implied distances, possibly accounting for the discrepancies seen in PNLF distances greater than 10 Mpc. Contamination of the PNLF by such objects has up to now not been seriously addressed. In this thesis, I explore a potential source of overluminous objects: planetary nebulae superimposed along the line of sight. Here, I present a reanalysis of the PNLF technique from the ground up to address this issue and determine whether blending is the primary source of systematic error observed in past PNLF studies. By analyzing 4 galaxies, I find that line-of-sight blending is very likely responsible for a significant portion of the apparent discrepancy between the PNLF and other methods at large distances.

Table of Contents

List of Figures

List of Tables

Acknowledgements

I would like to thank my thesis supervisor, Robin, for all of his patience and support throughout the process of completing this thesis. I would also like to extend my thanks to everyone else who has helped me both academically and personally as I have embarked on my research journey.

This thesis makes use of data from the Multi-Unit Spectroscopic Explorer (MUSE) instrument on the Very Large Telescope (VLT) operated by the European Southern Observatory (ESO). My analysis made extensive use of various Python libraries including Numpy (Harris et al., 2020), Matplotlib (Hunter, 2007), and Numba (Lam et al., 2015).

Chapter 1

Introduction

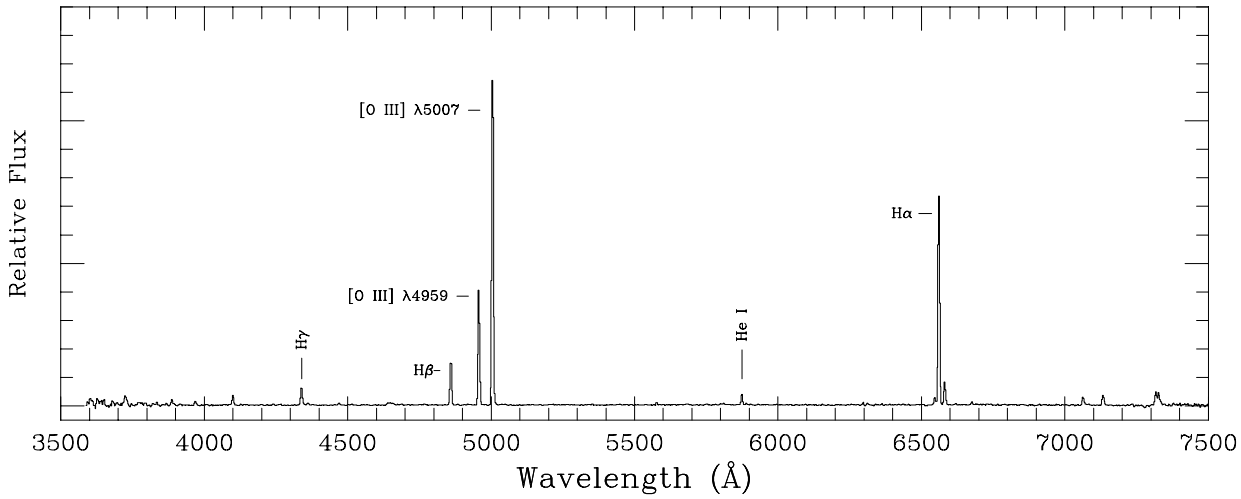

Figure 1.1: The spectrum of a typical planetary nebula with labelled emission lines. Notice the lack of appreciable continuum. Courtesy of Robin Ciardullo.

Planetary nebulae (PNe) are stellar remnants formed by $\sim$1-8 $M_\odot$ main sequence progenitors at the end of their lives (Kwitter & Henry, 2022). They consist of a gaseous nebula surrounding an extremely bright and hot central star. The central stars are among the brightest stars in a galaxy, reaching luminosities of $\sim$6000 $L_\odot$. However, these stars are also extremely hot, so most of this energy is emitted in the far-UV, often making them dim in the optical regime. The high energy emission of these stars ionizes the surrounding nebula, which re-emits the energy in a series of narrow emission lines. It turns out that the forbidden [O III] $\lambda5007$ line dominates this emission. In fact, up to 11% of the star's total emission can be accounted for by this single [O III] line (Schönberner et al., 2010). Therefore, PNe are easily identified via spectroscopic analysis. An example of a planetary nebula (PN) spectrum is shown in Figure 1.1. Note how the [O III] $\lambda5007$ and $\lambda4959$ lines are the dominant characteristics. Other relevant features include $H\alpha$ + the [N II] doublet and $H\beta$. It is also important to note that while galactic PNe are usually resolved (and are often the subject of beautiful Hubble Space Telescope images), extragalactic PNe are seen as mere point sources. This means that for all extragalactic purposes, we cannot observe anything about the structure of the nebula itself and can only identify them via their spectra.

Due to their dominant [O III] peak, PNe are easily distinguished from most other continuum

sources. This is classically done using a difference image technique which uses on-band and off-band photometry so that $\lambda 5007$ emission line objects stand out starkly against the continuum sources like stars (see Fig. 3 in Roth et al., 2021). And since the central sources of PNe are among the brightest stars in a galaxy, PNe themselves are visible in distant galaxies. In fact, individual PNe have been identified as far out as 100 Mpc (Gerhard et al., 2005). Given that their detection is relatively easy and they are very bright, PNe serve as important tools for extragalactic astronomy. PNe have been used extensively as indicators of galactic kinematics, serving as a probe for dark matter (Tian & Ko, 2016), constraining mass-to-light ratios (Aniyan et al., 2018), etc. Further, since PNe are so short-lived, they are excellent tracers for the current conditions of a galaxy. They can be used to understand properties of their progenitor stellar populations, such as metallicity (Galán-de Anta et al., 2021).

However, it is not single PNe that are of interest for extragalactic distances. Rather, it is when a galaxy's PNe population is viewed via its luminosity function (LF) that we are able to extract insight. A luminosity function is essentially a histogram which shows the number of PNe in a galaxy as a function of their (binned) brightness. Ciardullo et al. (1989) noticed that the planetary nebula luminosity function (PNLF) is well-fit by a powerlaw with a bright-end exponential cutoff, as in Equation 1.1, where the apparent magnitude, m, is given from the monochromatic $\lambda 5007$ flux (F_{5007} in [erg/cm^2/s]) by Equation 1.2. Note that in Equation 1.1 m^* is the apparent magnitude of the bright end cutoff, i.e., where the PNLF goes to 0. In Ciardullo et al. (1989), the authors obtained a calibration for the absolute magnitude of this cutoff: $M^* = -4.47$. They also argued that this cutoff could be exploited as a standard candle. The modern value for this absolute cutoff is -4.53 (Ciardullo, 2013).

$$N(m) \propto e^{0.307m}\{1 - e^{3(m^* - m)}\} \tag{1.1}$$

$$m = -2.5 \log F_{5007} - 13.74 \tag{1.2}$$

It is important to note that the relationship given in Equation 1.1 is purely empirical. There is no theoretical foundation supporting the existence of a bright end cutoff for PNe populations, nor is there theory to suggest that such a cutoff would be uniform across PNe populations, making it a standard candle. However, over the past 30 years, the PNLF has defied the limitations of our knowledge of stellar evolution. The PNLF has been shown to be a reliable standard candle impervious to galactic characteristics such as Hubble type, star formation rate (SFR), stellar mass, etc. (e.g., Ciardullo et al., 2002a; Feldmeier et al., 1997; Spriggs et al., 2021). Studies in M31 have been unable to discern any change in the cutoff even as a function of galactic radius (see Fig. 3 in Ciardullo, 2012). The only discernable variation in this bright end cutoff is in metal-poor populations. A falloff in the cutoff brightness in such populations is both predicted by models (Dopita et al., 1992) and has been observed (Ciardullo & Jacoby, 1992). This is not much of a problem, however, since there is a well-established positive relationship between a galaxy's stellar mass and its metallicity (Tremonti et al., 2004). Since PNe are fairly rare objects with lifespans on the order of $\sim$20,000 years (Badenes et al., 2015), low mass populations simply do not produce enough PNe for the LF to be well-measured. Not only are PNe themselves rare, but PNe in the top 1 mag of the LF represent only about 2% of all the PNe. This makes the bright end cutoff of low mass systems extremely hard to identify, so PNLF measurements would likely not be useful in such galaxies even if the dependence of the cutoff on metallicity was well-known. Due to this limitation, the PNLF has only been meaningfully applied to bright, massive galaxies for which the PN population is well sampled.

Since the introduction of the empirical PNLF given in Equation 1.1, others have suggested variations. For example, Longobardi et al. (2013) and Bhattacharya et al. (2019) both suggested subtle changes to the formula to account for variations in the slope at the dim end of the PNLF. However, as far as distances are concerned, most of the information is carried by the top 1-2 magnitudes of the PNLF, so such subtleties are not important. Further, questions of completeness arise at the faint end, meaning most of the dim planetaries observed in a galaxy are excluded from PNLF fits. There has also been work done on simulating PNe formation to generate numerical

PNLFs (e.g., Schönberner et al., 2010; Méndez et al., 2001). These often result in shallower slopes on the bright end, i.e., allowing brighter PNe. However, such simulations must make strong assumptions about the geometry of the nebular density and the initial mass function of the stellar population; choices for both of which are hard to just justify given very little evidence for their true distributions. Therefore, such simulations are not yet compelling enough to supercede the simple empirical formula of Equation 1.1.

As stated above, that simple formula has been remarkably successful as a robust distance indicator in the intermediate part of the distance ladder. However, certain limitations of the method have led it to be largely pushed aside in the past decade in favor of more fashionable methods such as the Levitt Law for Cepheids or the tip of the red giant branch (TRGB). The first and probably largest issue with the PNLF has always been the lack of theoretical background supporting it. Not only is there no theory to support the presence of the cutoff, there is also no theory suggesting that it should be identical across populations. On the contrary, intuition suggests that the cutoff should *not* be a standard candle. Ciardullo (2012) notes that from simple stellar evolution, the cutoff should change substantially over time, even as much as 4 mag over 10 Gyr. It is indeed quite surprising that early and late type galaxies would have the same cutoff. Another issue that makes this result even more unexpected is that PNe are known to have non-isotropic emission. Their dust envelopes do not have uniform densities; thus, the observed flux is geometry dependent. And this dust is very significant, causing an extinction in $\lambda 5007$ of at least 0.6 mag on average (Reid & Parker, 2010; Herrmann & Ciardullo, 2009). To further complicate the issue, Davis et al. (2018b) showed that when PNe are corrected for self-extinction, the PNLF looks very different. In fact, they show that the cutoff is likely a byproduct of self-extinction. All of this makes it very hard to trust the PNLF as a distance indicator from the get-go.

Even outside of the theoretical problems, the PNLF has faced other challenges. In late type galaxies, there are a variety of objects with the potential to contaminate the PNLF. Compact HII regions, supernova remnants (SNR), and even Lyα emitters (LAE) are all potential interlopers. Luckily, spectroscopic analysis is capable of reliably distinguishing these objects. Line ratios, such

as [O III] $\lambda 5007$ to Hα are significantly different between PNe and contaminants like HII regions, SNR, etc. (e.g., Herrmann et al., 2008; Davis et al., 2018a). These objects could have contaminated early PNLF studies that used narrow band interference filters, but newer, full spectrum data can immediately discriminate objects and correct distances accordingly (Kreckel et al., 2017).

Even with the elimination of contaminants, the PNLF has struggled to keep up in the race for accuracy in modern cosmology. The classic way of obtaining data for a PNLF study was to use interference filters on a 4-m class telescope (Ciardullo, 2012). Interference filters have rather poor spectral resolution and are difficult and costly to use with faster and bigger 8-m class telescopes. This has long held the PNLF back from reaching beyond 20 Mpc, far short of the mark necessary to compete today as a potential candidate to calibrate SNIa or directly probe the Hubble Flow. However, the introduction of integral-field unit (IFU) spectrographs has opened the door for the PNLF to make a comeback. Roth et al. (2021) outlines the advantages of such instruments. The authors demonstrate that the Multi-Unit Spectroscopic Explorer (MUSE) instrument on the Very Large Telescope (VLT) can be used to make PNLF measurements out to at least 40 Mpc. That study was done with data taken from the MUSE archive, which had significant limitations since the observations were not taken with the PNLF in mind. That leaves room to improve on this already incredible jump in the method's potential. This new technology sets the stage for the PNLF to reach cosmically significant distances and therefore, probe the Hubble Tension.

The Hubble Tension is perhaps the largest controversy in modern cosmology. It refers to the increasingly significant disagreement between measurements of the Hubble Constant, H_0, in the local universe (e.g., Riess et al., 2021; Freedman, 2021) when compared to those derived from early universe measurements (Planck Collaboration et al., 2020). Riess et al. (2021), which used Cepheids to calibrate SNIa, claims at least a 4σ disparity with the Planck measurements. Should the PNLF reach the capability to measure distances to a sufficient sample of bright galaxies out to $\sim$40 Mpc within about 5% accuracy, the method would be able to generate a value for H_0 with only $\sim$2% statistical error. This is certainly small enough to meaningfully contribute to the investigation of the apparent tension. Furthermore, the PNLF would be able to make such a determination of

H_0 independently of SNIa. Virtually no other robust method is capable of independently verifying SNIa measurements of distant galaxies. Thus, the door is open for the PNLF to step in as a cross check of the more fashionable rungs of the distance ladder. The only issues standing in the way of this goal are the lack of dedicated observations from modern IFU instruments like MUSE and the handling of potential systematics. As stated above, the PNLF has been questioned at distances greater than $\sim$10 Mpc due to the potential presence of such systematic problems. If these issues emerge at distances less than 20 Mpc, then it is imperative to thoroughly address them if the desired errors are to be achieved at twice the distance.

The goal of this thesis is to tackle the most pressing of the potential systematic problems with the PNLF: the apparent tendency for the PNLF to calculate shorter distances for relatively distant galaxies. Chapter 2 explores this potential offset in detail, as well as introducing various hypotheses regarding its origin, including the one which is tested in this thesis.

Chapter 2

Systematic Bias

2.1 History

In its 30 year history, the PNLF has demonstrated extraordinary agreement with Cepheid measurements out to $\sim$10 Mpc. This consistency is clearly seen in Figure 2.1, which shows all the galaxies measured with both methods. The residuals between the measurements for every galaxy are well explained by the quoted uncertainties in the measurements. A similar (yet inferior) consistency holds when PNLF measurements are compared to distances generated via the TRGB method. Not all the residuals with TRGB measurements can be accounted for by statistical scatter, but this is likely a result of the internal discrepancies between different TRGB measurements. Due to these well-established agreements, the PNLF has served as a useful cross-validation of these two trusted methods. In fact, calibrations of the PNLF cutoff using both the Levitt Law for Cepheids and the TRGB give values in excellent agreement (although the Cepheid calibration can vary depending on the choice of metallicity dependence in the period-luminosity relationship). Together, calibration from these two methods has resulted in a well-defined value for the PNLF cutoff to within about 5% accuracy: $M^* = -4.53 \pm 0.05$ (Ciardullo, 2013). Their agreement is very promising, since Cepheids are generally only found in young, star-forming populations, while the red giant branch tip is only well-defined in older stellar populations.

There have been studies which have suggested a possible discrepancy between the PNLF and Cepheids at further distances (Ferrarese et al., 2000). A similar issue has been observed between the PNLF and the TRGB, but there is also substantial scatter between individual TRGB measurements at such distances and there are issues with identifying the tip of the red giant branch in data. In both cases, the PNLF gives values less than its counterparts. However, these differences are rarely outside the expected errors in the measurements and do not carry enough evidence to imply a systematic error. The proverbial nail in the coffin for the PNLF came when it generated distances to the elliptical galaxies in the Fornax and Virgo cluster which were $\sim$0.2 mag shorter than those given by Cepheid measurements of the systems' spirals. This offset was further "verified" by SBF measurements in the clusters (Tonry et al., 2001), and it was concluded that the PNLF lacked the

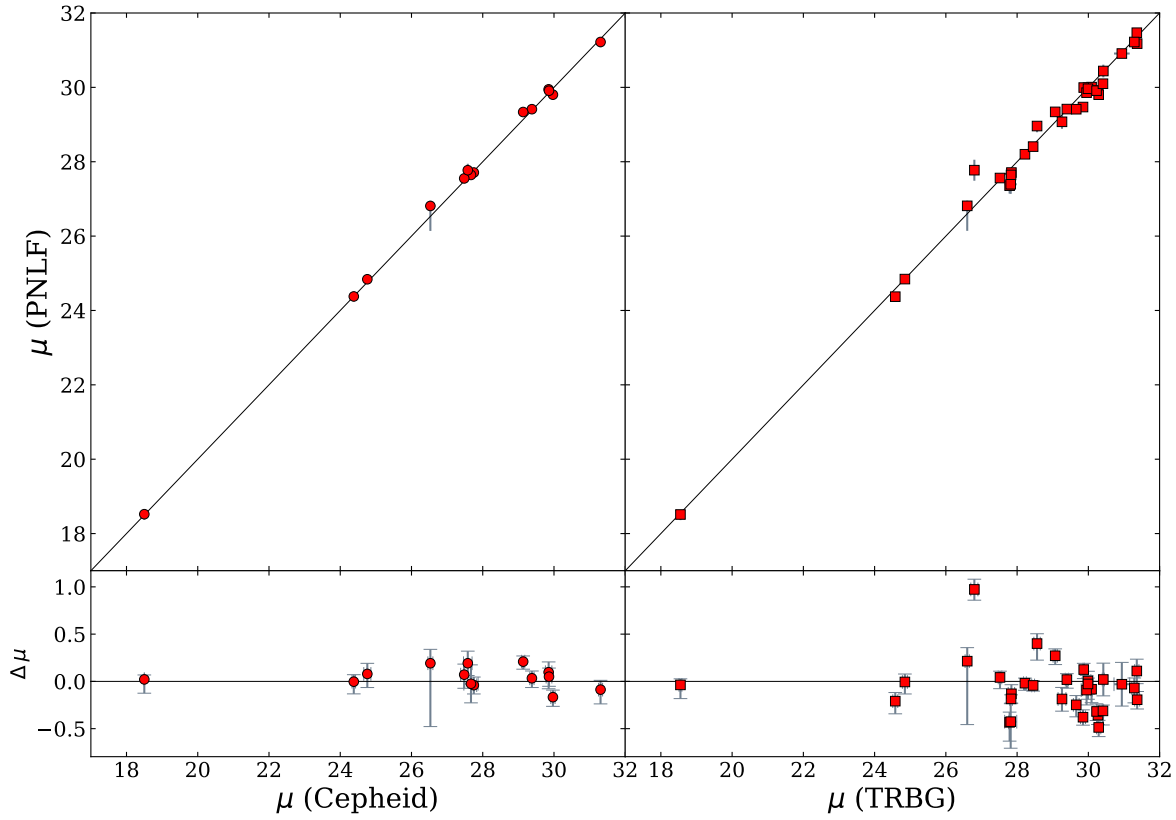

Figure 2.1: This plot compares the distances given by the PNLF with those given by Cepheids (left panels) and TRGB (right panels). The faint lines in all 4 plots show the 1:1 correspondence line. In the lower panels, the $\Delta\mu$ is given by computing μ(PNLF) - μ(other), so negative values indicate smaller PNLF distances. The PNLF demonstrates excellent agreement with Cepheid distances for all the galaxies measured with both methods. The result is less ideal for TRGB, but there is still good agreement. The PNLF distances shown here are from the following: Jacoby et al. (1990b); Ciardullo et al. (2002b); Jacoby et al. (1989); Hui et al. (1993); Ciardullo et al. (2004); Scheuermann et al. (2022); Feldmeier et al. (1997); Herrmann et al. (2008). The Cepheid distances come from: Freedman et al. (2001); Riess et al. (2016); Ferrarese et al. (2007); Macri et al. (2006); Saha et al. (2002). The TRGB measurements were obtained from either Beaton et al. (2016) or the Extragalactic Distance Database (Tully et al., 2009).

power to push into the upper rungs of the distance ladder.

In opposition to this view, Ciardullo et al. (2002a) argued that the offset with SBF distances could be well explained by uncertainties in the knowledge of the internal reddening of the observed galaxies. The reddening of any particular PN can be measured using the Balmer decrement, but in general, extinction which is a result of dust in our own galaxy and that from dust in the host galaxy are difficult to disentangle from the circumnebular dust of the PN itself. Such a differentiation is necessary based on the results of Davis et al. (2018b), which showed that the PNLF cutoff is likely a result of circumnebular material. Reddening inherent to the host galaxy has a nearly equal, but importantly, *opposite* effect on the distances using the PNLF and SBF. It only takes a very small mistake in the reddening estimation to account for the several tenths of a magnitude offset observed between the two methods. Ciardullo et al. (2002a) further argues that such an uncertainty in the reddening could be the result of differences in the populations contained in the nearby, late-type galaxies, which are used to calibrate both methods, and the early-type galaxies which are the more relevant, distant targets of SBF. It is difficult to observationally verify this argument; this is, in part, because it has thus far proven difficult to calibrate the PNLF within the Milky Way. Gaia distances are unreliable for PNe (González-Santamaría et al., 2021; Chornay & Walton, 2021), and once again, decomposing the components of the reddening is difficult.

Nonetheless, whether the PNLF/SBF discrepancy has merit or not, the PNLF assuredly has problems at large distances that must be addressed. This is apparent based on the plot in Figure 2.2, for which I have conglomerated the data from 48 distinct PNLF studies. All of the data has been shifted to absolute magnitude using the distance modulus implied for the respective galaxy. This is certainly not fool-proof; there are errors in the distance moduli and many of the objects in the overluminous tail were likely not included in the fits for those distance moduli. However, it goes to show that these objects are fairly common and challenges the notion of the PNLF cutoff as a standard candle.

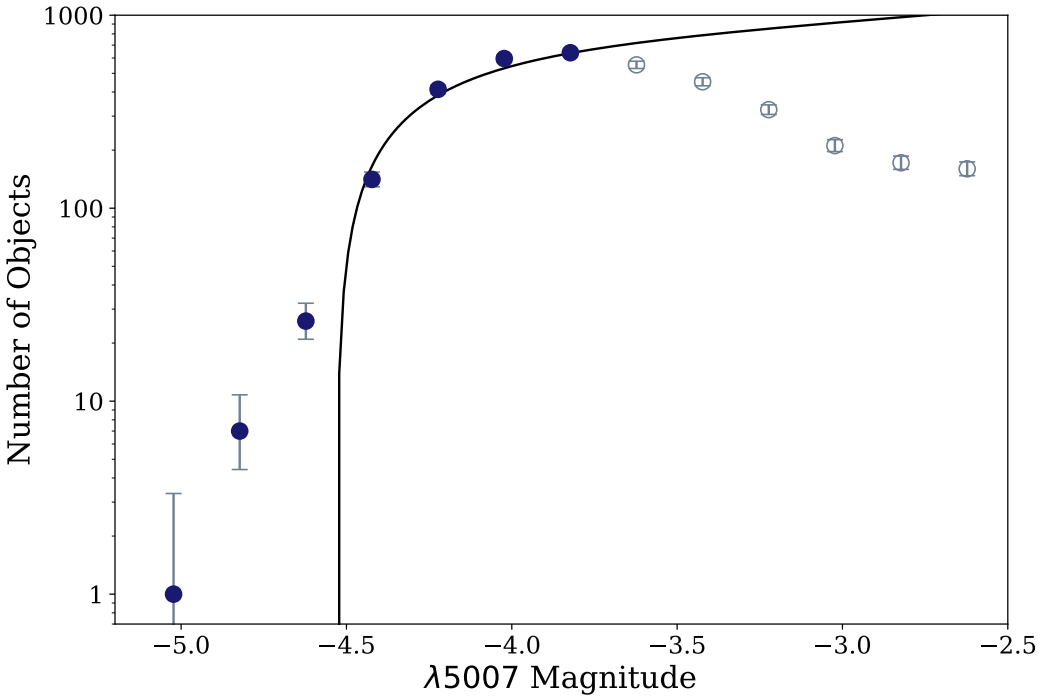

Figure 2.2: This plot combines the data of nearly 50 former PNLF studies in almost as many different galaxies. There are many overluminous contaminants of the PNLF, indicating that they may be rare but are certainly not an insignificant factor. The fit is simply the empirical model of Equation 1.1 with $\mu = 0$. Data courtesy of Robin Ciardullo.

2.2 Blending

A potential source of the observed offset (and general issue with the PNLF), which is also the primary subject of this thesis, are "overluminous" objects. Such objects are "overluminous" in the sense that they are too bright to be consistent with the rest of the data, assuming Equation 1.1 truly represents the population. The empirical form of the PNLF given in Equation 1.1 becomes identically 0 for $M < M^*$. That means that the apparent value for the cutoff, m^*, has to be at least as bright as the brightest PNe observed in a galaxy (within photometric errors). This has caused problems in computing the distances to some galaxies where there are one or two objects which, when included, make the empirical PNLF a very bad fit. When such objects are excluded, the cutoff generally fits the remaining data quite well. An example of such a situation is shown in Figure 2.3, which shows the PNLF histogram of M87 and an approximate implied PNLF fit from Jacoby et al. (1990a). M87 clearly has several objects that are not well explained by the exponential cutoff. These objects have appeared in the PNLFs of a variety of galaxies (including other in Jacoby et al., 1990a) and often appear 0.1 or more mags brighter than expected, based on the rest of the data. A 0.1-0.2 mag reduction in the measured value of m^* corresponds to a $\sim$10% reduction in the distance. Such extreme outliers are often excluded, which is not ideal, but if an object is only a few hundredths of a mag too bright, it could be impossible to identify. With no theoretical basis to work from, there is little to no understanding of these objects or their origins. Despite their enigmatic nature, these objects do present a ray of hope, as they are capable of producing the sort of offset that has thus far prevented the PNLF from reaching into the Hubble Flow. What's more, these objects have been most often seen when the PNLF has been pushed to its limits. As such, any modern use of the PNLF must address these objects to be at all competitive.

A number of possible explanations have emerged for these overluminous objects, and several have already proven inadequate. The natural guess would be contamination by non-PNe. However, as discussed in Chapter 1, these objects are much more of an issue in late-type galaxies, and there are ways to reliably distinguish common contaminants using spectroscopy. Problematic

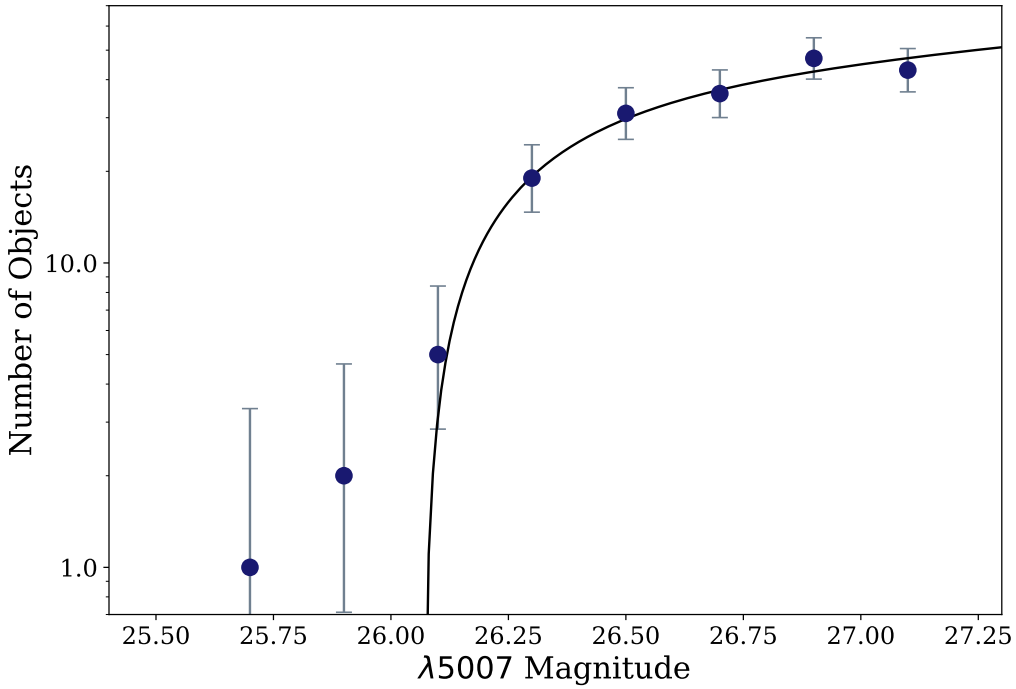

Figure 2.3: The PNLF of M87 using data from Jacoby et al. (1990a). The fit is based on the best distance found in that study. Notice that there are potentially 3 objects that can not be explained by the fit. The authors excluded these objects from the analysis because otherwise they would worsen the consistency with the majority of the data and shorten the distance by about 0.5 mag. If they were intracluster, they would require the Virgo cluster be abnormally stretched along the line of sight.

objects have been observed in early-type galaxies, and several have been spectroscopically confirmed as PNe (e.g., Roth et al., 2021). Another idea that has been suggested is that the objects are intracluster PNe foreground to the observed galaxy. While populations of intracluster PNe have been observed, this explanation also stands on shaky ground. Firstly, overluminous objects have been kinematically confirmed inside of galaxies (e.g., Sambhus et al., 2006); additionally, some objects in the Virgo and Fornax clusters would require the PNe be $\sim$2 Mpc closer than the observed galaxy. That would require a very strange elongation of the cluster along the line of sight. There is, of course, always the chance that these are a completely new breed of objects, but that is extraordinarily hard to argue since their spectra are completely consistent with those expected of standard PNe.

Another, and possibly the most likely, scenario is that these overluminous objects are the result of line-of-sight blending of two distinct PNe. Planetary nebulae are regions of diffuse emission with compact central objects. The nebular material is optically thin to the [O III] and Hα/β lines it produces since the oxygen lines are forbidden and the hydrogen is predominantly in the ground state, preventing Balmer absorptions. Therefore, if two PNe were lined up, there would be negligible eclipsing and their fluxes would, for all intents and purposes, add. A blend created by the overlap of 2, M^* PNe would be capable of producing an object with a measured absolute magnitude of -5.28 mag, a full 0.75 mag brighter than the individual objects. Naturally, such a blend would be extraordinarily unlikely, but it is not inconceivable that the overlap of two somewhat "average" PNe could result in an object appearing several tenths of a mag brighter than any other PNe in the galaxy. However, even PNe in the top 1 mag of the PNLF are somewhat rare. There may only be 20-30 such objects in a bright, large galaxy. It is natural to ask, then, whether these line-of-sight superpositions actually occur. Roth et al. (2021) demonstrated that the answer is emphatically yes, even using data from MUSE, which has the added advantage of being able to spectroscopically separate spatially blended PNe using the redshift difference in their $\lambda5007$ line due to their peculiar motions. In fact, that study was able to use spectroscopy to determine that an object deemed overluminous in a former PNLF study (which used simple interference filters) was

in fact spectrally separable. This is firm evidence that overlaps do occur and have contaminated past PNLF studies.

Clearly, the probability of confusing two objects as one depends on several factors including the seeing conditions and the density of PNe. This makes overlaps especially likely in the cores of galaxies where densities are high. Older PNe surveys generally avoided the cores of galaxies anyway, since poor signal-to-noise and partial object overlaps make doing anything difficult; however, modern, wide-field observations can often cover the whole galaxy. Also, recent instruments like MUSE often have small fields of view, so in order to see a relevant number of PNe, it is often necessary to observe nearer to the center of galaxies where there is more light. That hints at another advantage of solidifying the PNLF against overlaps because it would allow it to be used in worse seeing conditions leading to more galaxies and more PNe within galaxies being available for fitting. The task of the remainder of this thesis is to present a reanalysis of the PNLF which allows for line-of-sight superpositions. Chapter 3 explores the methodology behind such a reanalysis.

Chapter 3

Methods

3.1 Formal Treatment of Blends

In attempting to redesign the PNLF to account for the possibility of line-of-sight blending, it is not necessary throw out the empirical form of Equation 1.1. Rather, this analysis will proceed with the assumption that this is the true underlying distribution. Determining the shape of the observed distribution accounting for blends may seem like a tough task, but in fact, the formalism is not so complex. Firstly, the PNLF can be thought of as a probability distribution; that is, when properly normalized to 1, the functional value of a given bin times the bin size gives the probability of a random PN from the population falling in that bin. Let this normalized probability distribution take the form of Equation 1.1 and call it $\Phi(m)$. A line-of-sight superposition can be thought of as the addition of 2 randomly selected PNe from the population. When the distribution is converted to (linear) flux space ($\Phi(F)$), the distribution of the combinations of any 2 PNe at random is just the convolution of $\Phi(F)$ with itself. This can be expanded to any number of PNe. The distribution, ϕ_n, of the combined flux of n random PNe drawn from $\Phi(F)$ is simply the result of the convolution of n instances of $\Phi(F)$. Note that, in Euclidian space, the convolution is given by Equation 3.1 (Bracewell, 1999).

$$[f * g](t) = \int_{-\infty}^{t} f(\tau)g(t-\tau)d\tau \tag{3.1}$$

Given the distributions ϕ_n for all the possible number of overlaps, the observed PNLF, ϕ_{obs}, is simply given by the weighted sum shown in Equation 3.2. Note that this sum can be done in either magnitude or flux space as long as the convolution is done in flux space.

$$\phi_{obs} = \sum_{n=1}^{\infty} w_n \phi_n \tag{3.2}$$

The only things left to determine are the w_n terms which specify the relative probability of a given object being a result of n individual PN(e). Since the number of PNe in a given seeing area is a simple count, its distribution can be modelled as a Poisson distribution with mean given by the ex-

pected number of PNe in that aperture (as in Equation 3.3). In practice, the problem can be further simplified by ignoring the contributions of PNLF components for 3 or more blends. Not only are they a factor λ/n less likely for each successive number of overlaps, but at the distances/densities necessary for triple overlaps to be a significant factor in the total PNLF, it is probably not an especially accurate tool anyway.

$$w_n = Poisson(\lambda)[n] = \frac{\lambda^n e^{-\lambda}}{n!} \tag{3.3}$$

That expected count, λ, depends on a host of factors related to the observation itself, which implies that it is intrinsic not just to an individual galaxy but to every point in a galaxy. That is because the PNe in a galaxy "follow the light" in that their density is proportional to the underlying surface brightness (e.g., Coccato et al., 2009; Longobardi et al., 2013; Pulsoni et al., 2018). So, for every point in the galaxy, there is a unique λ which depends on the underlying surface brightness, the number of PNe per unit surface brightness, the seeing, and the size of the area (provided the area is small enough that the surface brightness is effectively constant throughout). The seeing relates to the ability to spatially discriminate close-by objects. Similarly, if the data contains spectroscopic information (as in the MUSE data used in Roth et al., 2021), there is also a term for the ability to spectroscopically discriminate overlapping objects due to their velocity separation.

It may seem that nothing has happened except kicking the can down the road. The value for the number of PNe per unit surface brightness might seem like a difficult quantity to know for a given population. However, it turns out that empirical evidence comes to the rescue once more, and the number of PNe in the top X mags of the PNLF, $\alpha_{X,PN}$, is generally constant across populations (Ciardullo, 2006). Further, even if it varies based on galactic characteristics, so long as it is constant within a given galaxy, it is a value which can be fit using the data. Also, any α_X can be scaled to any other α_Y using the ratio of the integral of Equation 1.1 from $-\infty$ to X to the integral from $-\infty$ to Y (so long as X is less than $\sim$1.5). This is potentially problematic since, as discussed in Chapter 1, the faint end of the PNLF has been observed to have different shapes in different populations. It is therefore advisable to include only the top few mags of the LF.

Calculating λ given α_{PN} is relatively straightforward. The expected number of PNe in a seeing unit should be the underlying bolometric galactic surface brightness times α_{m-lim}, where α_{m-lim} is α_{PN} scaled to the appropriate limiting magnitude of the observation. Then, simply multiply by the area of the seeing unit (telescope seeing squared). If spectroscopic information is available to differentiate blends by their velocity to some limit, Δv_{lim}, then there is another term as well. If the radial velocities in the galaxy can be approximated by a Gaussian distribution with dispersion σ_v, then the proportion of overlapped objects which cannot be spectroscopically differentiated is computable via the error function. Specifically, if a_{spec} is the fraction of doubled objects which cannot be separated by their velocities, then a_{spec} is computed via Equation 3.4. Note that the difference in the velocities of two PNe drawn from a Gaussian with mean 0 and standard deviation σ_v is distributed as a Gaussian with mean 0 and standard deviation $\sqrt{2}\,\sigma_v$.

$$a_{spec} = \text{erf}\left(\frac{\Delta v_{lim}}{2\,\sigma_v}\right) \tag{3.4}$$

When $\Delta v_{lim} \gg \sigma_v$, then we cannot differentiate any blends by velocity. Conversely, if $\Delta v_{lim} \to 0$, then our resolution elements are, in effect, infinitely small and there will be no apparent blends. In total, α times the surface brightness gives the expected number of PNe per unit angular area per spectral unit, and the seeing and a_{spec} are factors which modulate the size of a resolution element from both a spatial and spectroscopic perspective.

It is not entirely straightforward to determine Δv_{lim} from simple parameters like the spectroscopic resolution (usually quoted as an $R = \lambda/\Delta\lambda$ value). It depends on how confidently a fit of the line profile suggests a double-peaked shape. Thorough testing and calibration should be done for a given study to effectively estimate this value. One way of doing so is to generate artificial PNe and experiment with how often spatial blends can be identified via their velocity separation.

Since all the parameters related to resolution, PNe abundance, etc. combine into one number, they are all effectively degenerate. Therefore, it is possible to understand the effect of a change in any particular value constituting λ simultaneously by modulating λ itself. Any effect can be seen as either making blends more or less probable. The new form of the PNLF can be visualized by

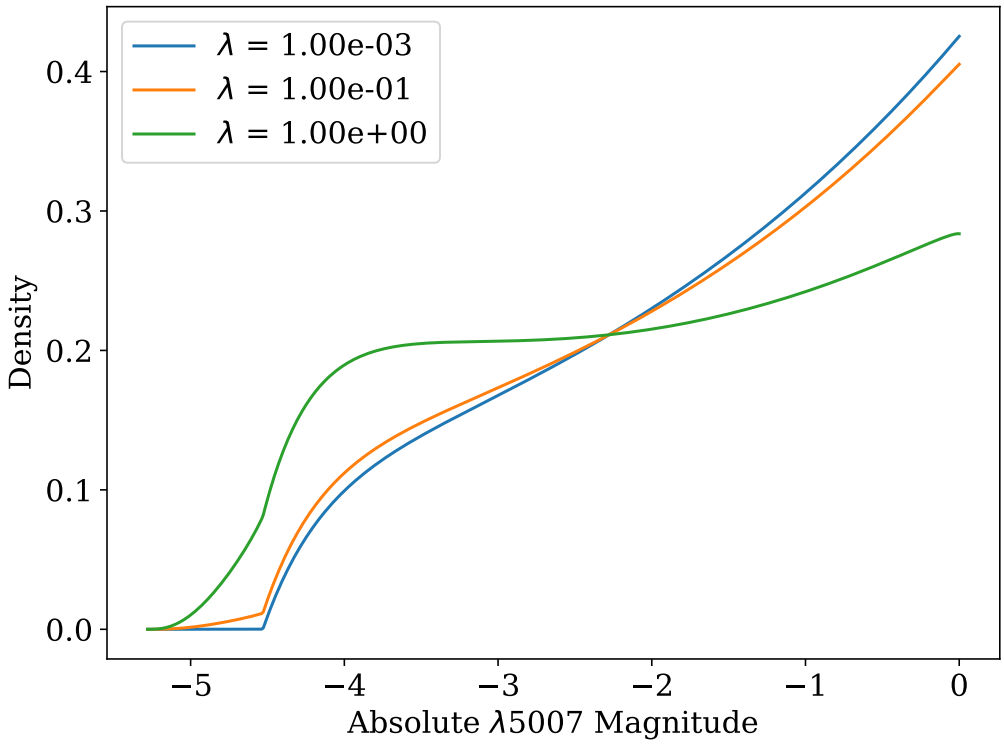

Figure 3.1: Example plots of the PNLF function with blends. For small values of λ (blue), the curve is virtually identical to the classic PNLF. As λ increases, a "foot" forms on the bright end which represents the allowance of PNe brighter than the empirical cutoff. The green curve shows an extreme case where λ is very large. The dim end appears to rise slower for higher λ, but this is a numerical effect due to the limits of the convolution (not going to 0 brightness). The bright foot connects to the rest of the curve via a sharp corner, but this is generally smoothed after convolving with the photometric errors.

simply specifying this one crucial value. Figure 3.1 contains several example PNLFs generated via this new formulation. Notice how, for small values of λ, the curve is effectively identical to the empirical form, but as λ grows, a sort of "foot" forms on the bright end where there is now probability associated with observing objects brighter than M^*. It is also important to notice that the PNLF still does go to 0 at $M = -5.28$. This is due to the fact that no individual PN is allowed to be brighter than M^* and thus no pair superimposed on each other can be brighter than the combination of 2, M^* PNe.

3.2 Simulations

With the new variable λ, which specifies the relative importance of the various PNLF components, introduced and defined, the stage is set to investigate whether overlaps are important from a theoretical perspective. The problem of determining the total probability of an overlap occurring in a galaxy mathematically is extremely difficult since each point of the galaxy has a different density of PNe and the number of PNe observed is itself a random variable. To avoid such complicated mathematical derivations, simulations can be used to generate approximate results with relatively little effort.

For example, a relevant question would be how likely an overlap is to appear overluminous given some inherent probability that an observed object is actually a superposition. To address this question, I created a simulation to randomly draw a sample of PNe magnitudes from the empirical law with the complication that with a specified probability, each sampled object magnitude would actually be the result of adding two random individual PNe magnitudes. By repeating this simulation for a variety of overlap probabilities, a general relationship between overlap probability and the chance of getting an overluminous object can be obtained. A plot showing the results of this simulation is shown in Figure 3.2. The interpretation of this plot is not entirely straightforward. Each simulation generated 100,000 object magnitudes where most were single PNe, but with the probability given on the horizontal axis, some were the combined magnitude of two random objects. The magnitudes were drawn from the top 4.5 mag of the PNLF. However, for calculating the fraction of overluminous objects, the total number of objects brighter than M^* was divided by the total number of objects brighter than $M = -3.5$. This is because the completion limit of PNLF studies is generally only 1-2 mags dimmer than M^*. Magnitudes down to 0 were included because PNe that would otherwise not be seen could boost a bright PN in the top mag of the PNLF over M^*. A linear fit of the data is also given in Figure 3.2. The trend is certainly not linear for the full range of overlap probabilities, but in general, probabilities greater than $\sim$0.1 are not relevant. In the concentrated regime shown in the plot from 0 to 0.1, the trend is somewhat linear. The implied

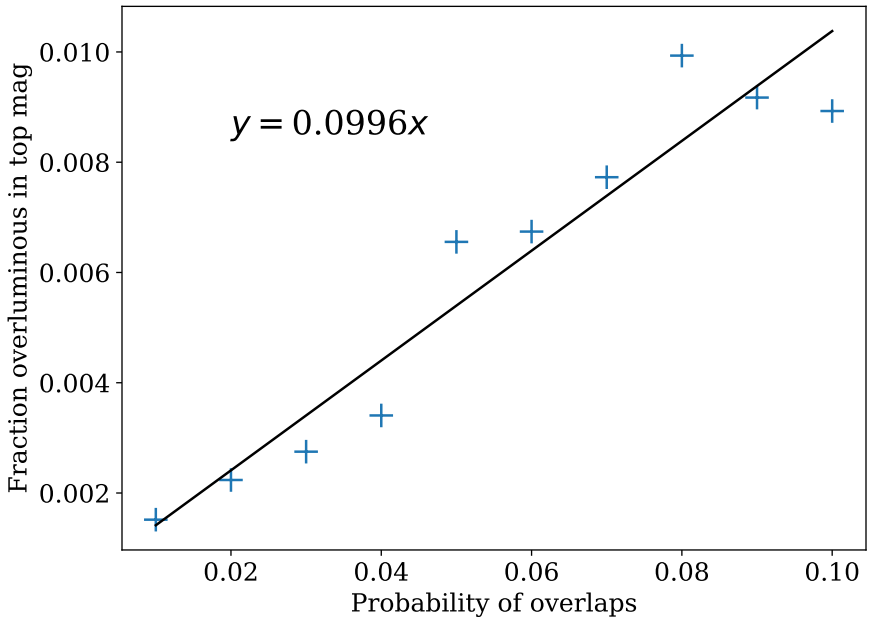

Figure 3.2: Plot showing the relationship between the frequency of overlaps and the frequency of overluminous objects. Each point summarizes a simulation wherein 100,000 PNe were sampled from within the top 4.5 mags of the PNLF. Some of the objects were the result of the addition of two objects. The probability of being overluminous was calculated as the fraction of objects brighter than $M = -3.5$ also brighter than $M^* = -4.53$. The equation on the plots is a simple linear fit of the data.

fit indicates a general rule: for small overlap probabilities, the fraction of objects in the top mag of the PNLF which will appear overluminous is $\sim$0.1 times that probability. Importantly, this does *not* mean that 10% of overlaps are overluminous, but just that if 1 in 10 objects is an overlap, then 1% of all observed objects (at the top of the PNLF) will be overluminous. Note that the seemingly large scatter in Figure 3.2, despite each point representing a 100,000 object simulation, is because only a small fraction of those 100,000 objects fall in the top mag of the PNLF and are included in the calculation of the relevant fraction.

The next question that arises after considering how overlaps relate to overluminous objects is how λ, which is a calculable quantity, relates to the probability of observing an overlap. To approach this problem mathematically, recall that λ can be interpreted as the Poisson mean number of PNe observed in a resolution element. The probability of an overlap should be the probability

that more than 1 object is observed divided by the probability that at least 1 object is observed. This is because we are not interested in resolution elements that do not contain any planetaries; rather, we are interested in the proportion of objects we observe which turn out to be two superimposed planetaries. This is simply calculated from the probability mass function of the Poisson distribution. The result is given in Equation 3.5. For small values of λ, that equation can be further simplified into Equation 3.6. This is easily recognized as the probability that a Poisson random variable with mean λ is greater than 0. This may seem strange, but it is a result of the fact that when the Poisson distribution is renormalized such that $N > 0$, then $N = 1$ effectively takes the place of $N = 0$ so long as the mean is small.

$$P = 1 - \frac{P(N = 1)}{1 - P(N = 0)} = 1 - \frac{\lambda e^{-\lambda}}{1 - e^{-\lambda}} \tag{3.5}$$

$$P = 1 - e^{-\lambda} \tag{3.6}$$

The problem can also be approached via simulation. Simulating a large area with a constant value for λ involves creating a large box which contains many resolution elements and randomly dropping PNe into the box. Since the expected number of resolution elements necessary to see 1 PN is $1/\lambda$, to get N PNe on average the box needs to have an area of N/λ. I conducted such a simulation in which I randomly placed 100,000 PNe in a box with size determined by N and λ. There should technically be some scatter in the number actually present, but this effect is not important when investigating the average probability of an overlap given a certain value for λ. The other important note is that to assess the probability of an overlap, it is not correct to divide the number of instances of overlaps by 100,000. Rather, we are interested in the proportion of overlaps to the number of objects, where two overlapping PNe constitute just one object. So, for each overlap, the total number of objects must also be decreased by one. Running such a simulation over many values of λ and counting the number of overlaps in each resulted in the data plotted in Figure 3.3. I also plot Equation 3.6 over the data. Notice that the expected equation works well at very small

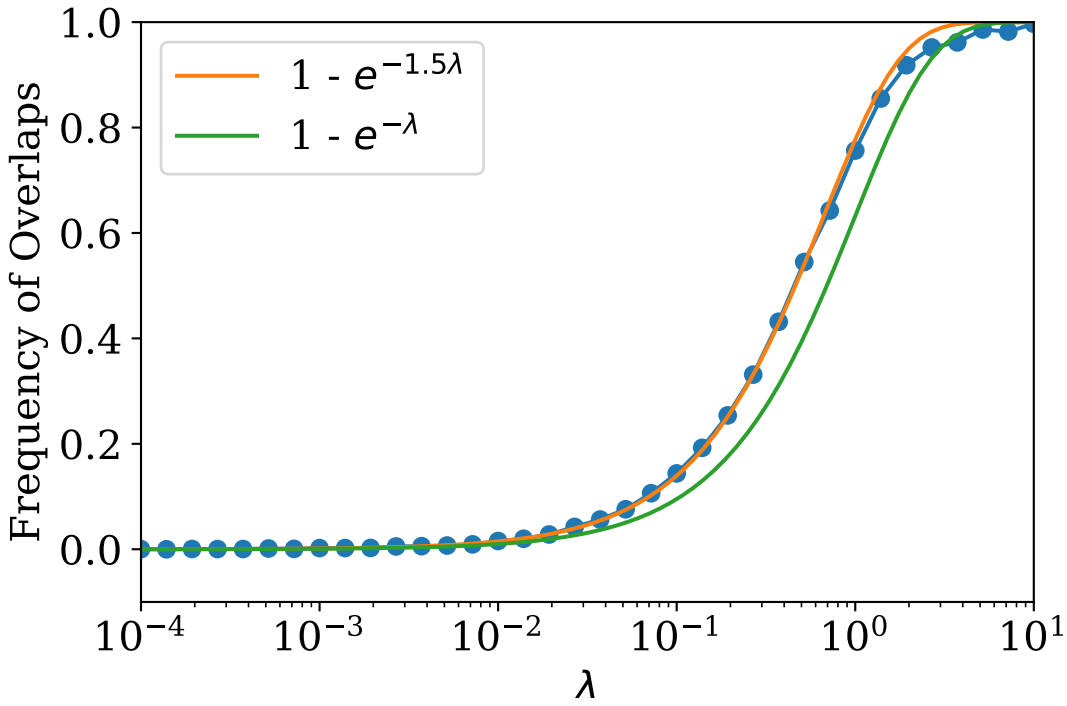

Figure 3.3: Plot demonstrating the relationship between the new parameter, λ, and the proportion of observed objects which are overlapped. The green line is what might be expected from a mathematical standpoint, but the orange line is a slight shift to fit the simulated data in blue. Each blue point is the result of placing 100,000 objects into a box defined by the parameter. The orange function is an excellent fit to about $\lambda = 1$, which is plenty far for application to any realistic data.

λ but quickly develops a bias and under-predicts the frequency of overlaps. Since the shape looks good, I attempted to shift the curve left by multiplying the variable by a constant. The constant which turned out to work quite well for fitting the data is 1.5. The plot of that curve is also shown in Figure 3.3. I hypothesize that the 1.5 inflation of the actual λ value is a result of several factors. Firstly, sometimes PNe occur in chains forming an extended object. The third PNe to join a chain does not increase the number of overlapped objects, but does decrease the total number of objects. Also, there is likely an increase in the number of overlaps when many resolution elements are tessellated together since PNe in adjacent elements which are populated by just 1 PN each could overlap with each other, despite the fact that each of their respective elements does not contain more than one object.

To get a general idea of how the information in Figures 3.2 and 3.3 relate, Table 3.1 shows

λ	Prob. Overlap	Prop. overluminous*
10^{-4}	1.5×10^{-4}	1.5×10^{-5}
10^{-3}	1.5×10^{-3}	1.5×10^{-4}
0.01	0.0148	1.48×10^{-3}
0.05	0.072	0.007
0.1	0.14	0.014

Table 3.1: Example values for λ and the corresponding probabilities for an object to be an overlap and proportion of objects (*in the top 1 mag of the PNLF) which appear overluminous. Note that for the small values of λ relevant to this study, the probability of overlap is very close to $1.5 \times \lambda$. The final column is approximated using the relationship established in Figure 3.2. These numbers serve to show how relevant overlaps can become. For $\lambda = 0.01$, already more than 1/100 objects are overlaps and 1/1000 at the top of the PNLF will be overluminous on average.

some example values. With this information, it is possible to test that the reformulation given in Section 3.1 works as intended. To do this, I once again simulated PNLFs by drawing from the empirical formula while having some chance of an object being the combination of two samples (as in Figure 3.2). By plotting the resultant simulated PNLFs with a numerical PNLF generated by assuming a value for λ, it is possible to see how well the new PNLF works. Examples of such plots are shown in Figures 3.4 and 3.5. They clearly demonstrate that the reformulation of the PNLF presented in Section 3.1 is accurately accounting for the effects of possible blends.

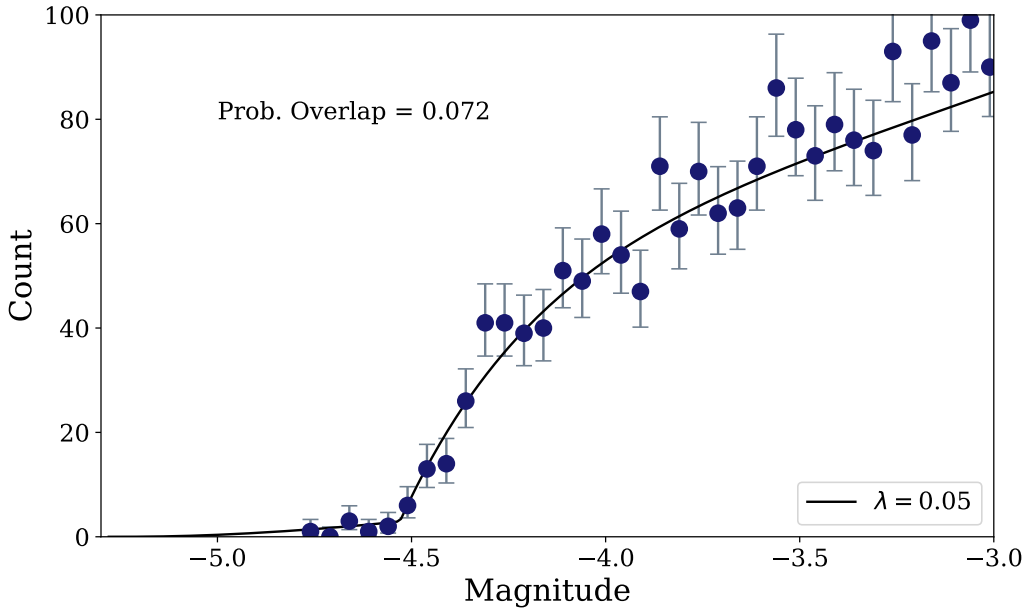

Figure 3.4: Blended PNLF for $\lambda = 0.05$ plotted over a simulated PNLF with an overlap probability of 0.072. The function (which is not a fit) describes the data well. The couple of overluminous objects that appear are well accounted for in the "foot" of the PNLF function.

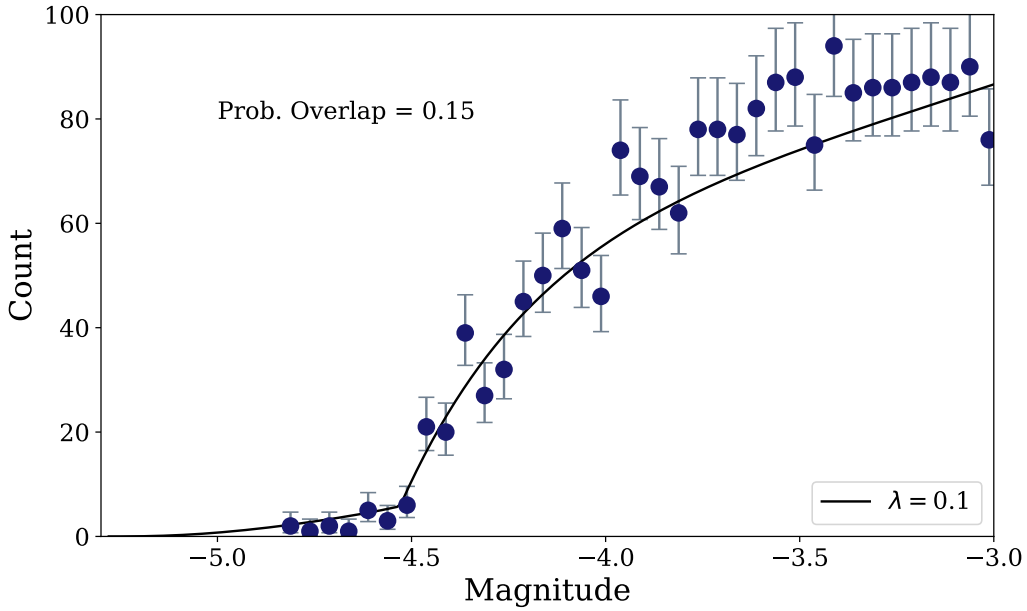

Figure 3.5: Blended PNLF for $\lambda = 0.1$ plotted over a simulated PNLF with an overlap probability of 0.15. The function again describes the data well. This value of λ is likely unrealistic, but it serves to illustrate the effectiveness of the new formulation of the PNLF.

3.3 Maximum Likelihood Fitting of the Luminosity Function

The most accurate and robust way to fit a luminosity function is via the maximum likelihood method, as introduced in Hanes & Whittaker (1987). Such a fitting is independent of arbitrary choices regarding binning and has been used extensively for the PNLF (Ciardullo et al., 1989). However, since this new formulation of the PNLF specifies that each PN should have a unique PNLF, this fitting procedure must be updated.

In a given observation, we observe a luminosity function for a whole galaxy, $\Phi(M)$, down to some limiting magnitude, m_{lim}. We consider this galactic luminosity function to be a result of individual luminosity functions manifested at each point in the galaxy. Specifically, we have a different luminosity function, ϕ_i, for every PN we observe. Our goal is to fit the observed luminosity function by maximizing the likelihood of observing the data given the model, which is a function of distance and PNe abundance.

If we view $\Phi(M)$ as a probability distribution, then the expected number of PNe in a given bin of the luminosity function will be $E(n)_M = T\Phi(M)dm$, where T is some normalization constant. However, we can also split $\Phi(M)$ into its component underlying luminosity functions ϕ_i such that the expected number of PNe in a given bin is the sum of the expected number of PNe in the same bin over every ϕ_i. The expected number in a bin of a single ϕ_i is given by the probability distribution times the abundance of PNe at that location, λ_i, as in Equation 3.7. Recall that λ_i is a function of the underlying surface brightness, the number of PN per unit surface brightness, α_{PN}, and some parameters of the observational setup. Summing these expectations for every component PNLF (ϕ_i) gives the expectation for the total number of PNe observed in that bin. This total expectation formula is given in Equation 3.8.

$$E_i(n)_M = \lambda_i \phi_i(M) dM \tag{3.7}$$

$$E(n)_M = T\Phi(M)dM = \sum_{i=1}^{N} \lambda_i \phi_i(M) dM \tag{3.8}$$

The number of PNe actually observed in a given bin of a particular ϕ_i is distributed as a Poisson random variable with mean given by the expected value given in Equation 3.7. The number observed in that bin for the whole galaxy is then the sum of those random variables. The sum of Poisson random variables is itself a Poisson random variable with mean given by the sum of the means of the constituents. Therefore, the probability of observing n PNe in a given bin is given by Equation 3.9 (which is simply the Poisson probability mass function).

$$P(n)_M = \frac{(\Phi(M)dM)^n * e^{-\Phi(M)dM}}{n!} \tag{3.9}$$

The total probability of a given observation is the product of probabilities for each bin. Letting the bin size go to 0, each has either 0 or 1 object (single PN or blend of two). Therefore, the total probability of a PNLF candidate fit takes the form of Equation 3.10. That equation can be rearranged since the exponential is common to both factors giving Equation 3.11.

$$P = \prod \left[(E(n)_M)^0 * e^{-E(n)_M}/0! \right]_{n=0} * \prod \left[(E(n)_M)^1 * e^{-E(n)_M}/1! \right]_{n=1} \tag{3.10}$$

$$P = \prod_{M=-\infty}^{M=M_{lim}} \left[e^{-E(n)_M} \right] * \prod E(n)_{M\, n=1} \tag{3.11}$$

Working with log-likelihoods is computationally easier, so Equation 3.11 can be improved by taking the natural log of both sides. Equation 3.8 can also be used to replace $E(n)_M$. This results in the messy looking Equation 3.12.

$$\log P = -\sum_{M=-\infty}^{M_{lim}} \left[\sum_{i=1}^{N} (\lambda_i \phi_i(M) dM) \right] + \sum_{j=1}^{N} \left[\log \left(\sum_{i=1}^{N} (\lambda_i \phi_i(M_j) dM \right) \right] \tag{3.12}$$

To simplify the expression for $\log P$, dM can be pulled out of the inner sum in the first term. This

generates a constant N, the number of PNe observed in the galaxy, but allows the outer sum to be viewed as an integral when $dM \to 0$. The dM factor in the second term can also be extracted from the sums. These adjustments result in Equation 3.13.

$$\log P = -N \int_{-\infty}^{M_{lim}} \left[\sum_{i=1}^{N} (\lambda_i \phi_i(M)) \right] dM + \sum_{j=1}^{N} \left[\log \left(\sum_{i=1}^{N} \lambda_i \phi_i(M_j) \right) \right] + N \log(N * dM) \tag{3.13}$$

The last term can be ignored since it is constant as a function of distance and α_{PN}, and only relative likelihoods are important. So, the final expression for $\log P$ that can be used to compare various model fits is shown in the mildly simplified form of Equation 3.14.

$$\log P = -N \int_{-\infty}^{M_{lim}} \left[\sum_{i=1}^{N} (\lambda_i \phi_i(M)) \right] dM + \sum_{j=1}^{N} \left[\log \left(\sum_{i=1}^{N} \lambda_i \phi_i(M_j) \right) \right] \tag{3.14}$$

Implementing this probability function is significantly more complicated than that of the former PNLF formulation. That is because rather than building just one PNLF for a galaxy, N different PNLFs have to be constructed and the density values of all N PNe computed for each. The likelihood function is a non-trivial combination of these many values and is a function of just two external parameters: distance modulus, $(m - M)$, and PNe abundance, (α_{PN}). Any maximization technique can be applied to this function to determine the best fit values for given data, although the derivatives of Equation 3.14 with respect to the parameters are generally intractable, so methods like Levenberg-Marquart are not advisable.

Chapter 4

Results

4.1 Data

For this thesis, I use the new formulation of the PNLF which incorporates blends on 4 test galaxies: the Antennae Galaxies, NGC 1399, NGC 1351, and NGC 1512. Among these test cases, only NGC 1399 and NGC 1351 have been previously measured with the PNLF. The details regarding each galaxy will be given in their respective sections.

The data I use in this thesis are from the MUSE archive. Identification of PNe and photometry were done by Martin Roth in the same manner as in Roth et al. (2021). The data includes $\lambda 5007$ magnitudes with photometric errors and underlying surface brightness values for every single PN identified in the data cube. I process this data in a Python program I wrote which implements the algorithm described in Chapter 3.

The method I use to fit the two parameter model given the likelihood function in Equation 3.14 is a naive grid search over both parameters. Other implementations are possible, including the popular Markov Chain Monte Carlo (MCMC) method, and further work could be done to make the fitting computationally less expensive while more thoroughly sampling the parameter space. I additionally fit the same data using the classical form of the PNLF (without blending) to see the comparison. I do so in the style of Ciardullo et al. (1989). The errors I quote on my fits are only the statistical errors on the fits, and future work is required to thoroughly assess the possible systematic errors from the reddening, PNLF calibration, photometry, etc. In fact, since the MUSE data were not taken under ideal circumstances for use with the PNLF, there are likely such systematics associated with things like the aperture correction which affect the fits. Worse still, these systematics could be different for every pointing in the galaxies. Since MUSE has a small field of view of just $1' \times 1'$ (Bacon et al., 2010), each galaxy's PNLF is constructed from several different pointings, all with potentially different systematic uncertainties/issues.

The error bars included on the PNLF histograms for each galaxy (and for the relevant figures earlier in this thesis) are the 68% confidence interval bounds for a Poisson random variable, computed using the recommended approximations (Eqns. 7 and 14) in Gehrels (1986). These are not

the same as the simple $\sqrt{N}$ errors given by the central limit theorem Gaussian approximation, which requires large N. Another important detail for the plots in this section is that the blended PNLF is very hard to visualize. Since it is different for every PNe in a galaxy, there is no "right" way to plot it on the PNLF histogram for the galaxy as a whole. Therefore, I simply plot the standard empirical PNLF placed at the distance computed using blends. This may happen to appear to be a bad fit in certain cases, but that is just a matter of the visualization.

All of the PNLF fits are calculated on the original, reddened data. The distance modulus is then dereddened using the $\lambda 5007$ extinction given by $A_{5007} = 3.47 \times E(B-V)$ (Cardelli et al., 1989). I adopt the reddening values of Schlafly & Finkbeiner (2011). There is the minor caveat that for the blended fits, the surface brightness values are dereddened before being used to compute λ. Another important parameter for each galaxy is the general velocity dispersion. In the MUSE data, PNe that are spatially overlapped can be reliably distinguished spectroscopically so long as their radial velocity separation is greater than about 100 km/s. I therefore employ 100 km/s as the velocity resolution used in computing the λ values. The issue of velocity dispersion for each galaxy is more complicated since velocity dispersion is, in general, a function of galactic radius, and thus different for every object. Rather than attempt to compute a local velocity dispersion for every object, though, I adopt a "typical" value for for the galaxy and apply that uniformly across the PNe. The effect of such an approximation is exceedingly small and rigorous enough for the scope of this thesis. In the future, this effect should be explored to ensure the smallest possible systematic errors.

4.2 Antennae Galaxies

The Antennae Galaxies are a pair of spiral galaxies currently undergoing collision. The interaction is causing the combined object to undergo rapid star formation. They are an interesting target for the PNLF because it represents another test of its consistency, this time in an irregular galaxy (pair) with rapid star formation. The distance to the Antennae is relevant because it does not have a large set of reliable measurements. Not being in a major cluster, it is only the direct distance that can be used to obtain luminosities within the galaxies and thereby derive parameters like stellar mass.

In 2007, the Catalina Sky Survey observed a SNIa (SN2007sr) in the Antennae. This drew interest to the galaxies which had previously been measured almost exclusively via the Tully-Fischer Relation. Riess et al. (2011) used SN2007sr with a calibration of the SNIa peak magnitude by Cepheids to compute a distance modulus of 31.66 ± 0.08 (21.48 Mpc). However, other distances published using the supernova span more than a full magnitude. Jang & Lee (2015) obtained a distance modulus of 31.67 ± 0.05 (21.58 Mpc) using the TRGB, which is in good agreement with the SNIa measurement.

The MUSE data for the Antennae contain 251 total PNe. However, the sample is only complete out to 28.5 mag, leaving the complete sample with 138 PNe. The literature contain no measurements of the Antennae's velocity dispersion, but there was a recent hydrodynamical simulation of the merger presented in Lahén et al. (2018). They report a radial velocity dispersion curve from which I estimate a representative value of 150 km/s over the region of the MUSE pointings. Given a reddening of E(B-V) = 0.0398, I found the best fit value with blends to be $(m-M)_0 = 31.84^{+0.05}_{-0.06}$ (23.3 Mpc). Without blends, the value shrinks to $(m-M)_0 = 31.75^{+0.03}_{-0.05}$ (22.4 Mpc). The blended PNLF extends the distance by nearly a tenth of a mag. Figure 4.1 shows the two fits on the PNLF histogram. The first thing to notice about Figure 4.1 is that the construction with blends has done exactly what it was intended to do. The black curve appears to have pushed the distance closer than ideal in order to appease the brightest PN, while the yellow fit seems to largely adhere to the

bulk of the data better. The distances I have computed may seem out of line compared to the SNIa and TRGB measurements quoted above, but the difference is really not so extreme considering I only consider statistical errors and these MUSE data are sub-par on account of coming from the archive.

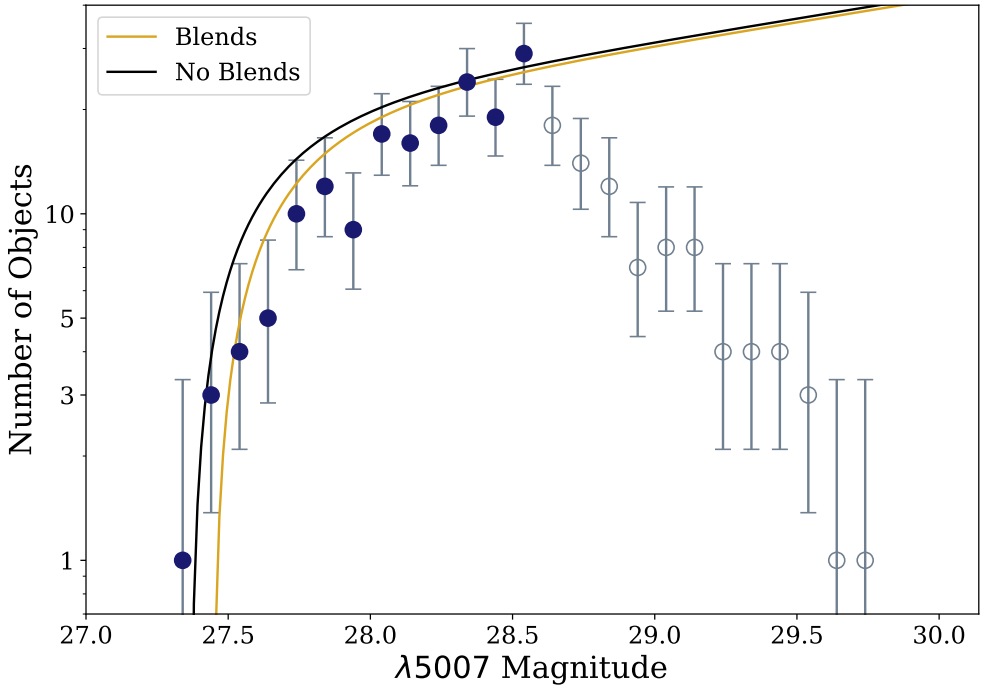

Figure 4.1: This plot shows the PNLF (0.1 mag bins) and fits for the Antennae galaxies. The yellow curve is the empirical PNLF plotted at the distance modulus computed using blends. The black curve is the fit for the empirical PNLF plotted at the distance it computes itself. Note that the black curve does seem to be drawn away from the majority of the data by one bright PN. The blended PNLF seems to correct for this effectively.

4.3 NGC 1399

NGC 1399 is a very large elliptical galaxy and the central dominant (cD) galaxy of the Fornax cluster (de Vaucouleurs et al., 1991). As such, it has been the target of a substantial number of distance studies; however, the galaxy has not been measured using Cepheids, TRGB, or SNIa since it is an early-type galaxy with little to no star formation and no observed SN. This makes it interesting in almost the exact opposite way as the Antennae. A quality PNLF distance to NGC 1399 could help set the method up as the best bridge between early- and late-type distance indicators. Of course, the distance itself is interesting in that it helps define the distance to the whole host of galaxies in the Fornax cluster. There is a prior PNLF distance for the galaxy from McMillan et al. (1993): $(m-M)_0 = 31.17^{+0.05}_{-0.07}$ (17.1 Mpc). In comparison, the most recent SBF measurement gives $(m-M)_0 = 31.596 \pm 0.091$ (Blakeslee et al., 2009). The Cosmicflows-2 dataset yields a "statistical" distance of $(m-M)_0 = 31.72 \pm 0.12$ (Tully et al., 2013). The PNLF distance is quite old, but does follow the trend of being short of the distances generated by these other methods by a fair margin.

In its MUSE pointings, there are 232 identifiable PNe spanning apparent magnitudes from 26.7 through 29. The complete sample extends to 28 mag and contains 180 objects. For the velocity dispersion, I approximated a "typical" value of 275 km/s for the relevant portions of the galaxy based on the kinematic results in Saglia et al. (2000). Assuming E(B-V) = 0.0109, the best fit distance using the new PNLF is $(m-M)_0 = 31.38^{+0.04}_{-0.03}$ (18.9 Mpc). Without blends, the PNLF distance shrinks to $(m-M)_0 = 31.19^{+0.04}_{-0.05}$ (17.3 Mpc). This is an interesting result, in that the "standard" PNLF distance is extremely similar to the 1993 value, and the result incorporating blends extends the distance about 0.2 mag, leaving it still slightly short of the other methods. There are complications, though. The PNLF for NGC 1399 does not look great to begin with. The histogram in Figure 4.2 is relatively strange because it seems to jump in ways that I would not expect. This is very likely a result of the non-ideal nature of the data, specifically the variations in systematics between different pointings. This certainly factored into the fitting, as the distance with

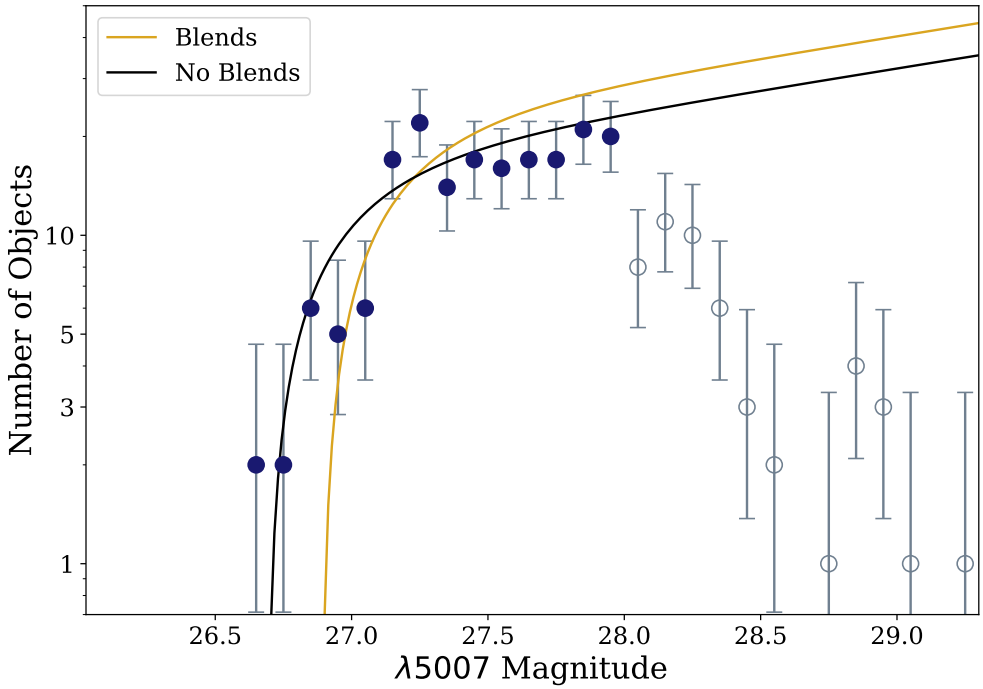

Figure 4.2: The PNLF of NGC 1399 (0.1 mag bins). The black fit was generated without allowing for blends, while the yellow represents the blended fit. The blended fit may appear poor, but the plot is not the actual best fit function, rather just a visualization of the standard function shifted to the distance computed with blends. The blends have clearly had a large impact on the fitting for this galaxy.

blends was not very stable to changes in the input parameters, especially α. The plot in Figure 4.2 shows that the blended distance also requires that many of the PNe be overluminous. The galaxy is very bright and sits in the middle of a large cluster, so this is not entirely strange, but the large velocity dispersion makes this questionable.

4.4 NGC 1351

NGC 1351 is a smaller elliptical galaxy in the Fornax cluster. It offers the opportunity for validation with NGC 1399. Similar to NGC 1399, it only has prior distances from methods that are effective on early-type galaxies like SBF and Tully-Fischer. It does have one PNLF measurement, made by Spriggs et al. (2021) using the same MUSE data. Their best fit value was $(m-M)_0 = 31.34^{+0.14}_{-0.15}$ (18.5 Mpc). Blakeslee et al. (2009) also measured NGC 1351 (using SBF), obtaining a distance modulus of $(m-M)_0 = 31.422 \pm 0.071$ (19.23 Mpc). Similarly, Cosmicflows-2 also has a distance generated by combining previous results: $(m-M)_0 = 31.42 \pm 0.12$. Note that the distance from Blakeslee et al. (2009) probably plays a large role in the Cosmicflows distance, explaining their close agreement. The distances to NGC 1351 are somewhat similar, albeit decidedly shorter than those to the cD galaxy, NGC 1399.

The MUSE data contain 102 PNe, of which 56 are brighter than the apparent completion limit of 28.1 mags. The central velocity dispersion was measured as $\sim$150 km/s by Vanderbeke et al. (2011). Since the velocity dispersion is expected to fall with radius, I assume a value of 100 km/s as an estimate for the regions with PNe observed by MUSE. With a reddening of E(B-V) = 0.0115, the blended distance to NGC 1351 that I compute is $(m-M)_0 = 31.40^{+0.06}_{-0.13}$ (19.0 Mpc). This is an extension from the no-blends fit, which gives $(m-M)_0 = 31.25^{+0.05}_{-0.7}$ (17.8 Mpc). The blended PNLF has once again done an excellent job extending the classic PNLF distance, which is several tenths of a mag short of other methods, into agreement with those methods. This difference can be seen in the PNLF plots in Figure 4.3. Interestingly, the new PNLF distance disagrees with the pattern between NGC 1399 and NGC 1351 observed by other methods. The cD galaxy appears to be behind NGC 1351 by $\sim$2.5 Mpc based on other methods, but the blended PNLF results presented here put the two galaxies at almost the same distance. This once again points to issues with the NGC 1399 data. The no-blend distance I found is slightly less than that given by Spriggs et al. (2021), although it is within their 1σ lower error. With proper analysis of systematics, their value would likely be within the upper error of my measurement.

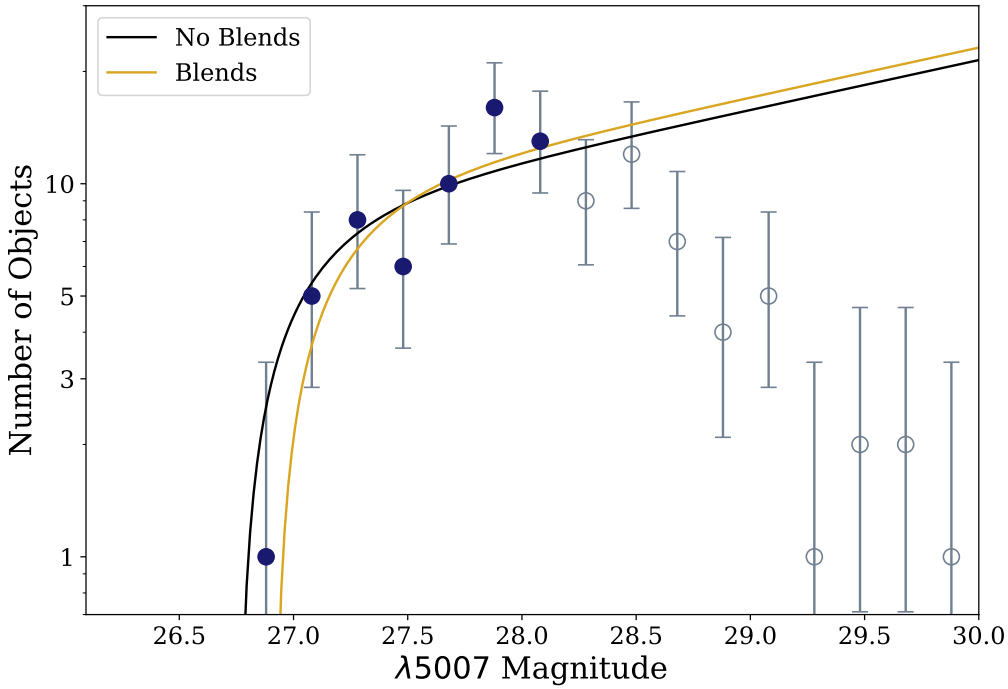

Figure 4.3: The PNLF (0.2 mag bins) and fits for NGC 1351. Once again, incorporating blends extends the distance from the classic PNLF technique, this time by ~ 0.15 mag. I have plotted the curve representing the blended fit with a higher normalization to better reflect the data.

Take note of the large lower error on the blended measurement. The likelihood distribution does in fact show excess probability on the left side, probably related to the probability peak in the no-blends case. This is not an unexpected result. In fact, the likelihood distribution for fits with blends can often turn out to have several distinct peaks since the size of the foot on the blended PNLF density function increases at larger proposed distances.

4.5 NGC 1512

NGC 1512 is a large, face-on, barred spiral galaxy in the Dorado Group. It has an HI disk extending far beyond its optical radius and has extensive star formation in both the optical and HI disks (Koribalski & López-Sánchez, 2009). However, it is not one of the brightest galaxies in the group (which also contains NGC 1566, 1553, and 1549), so it attracts generally little attention. Past measurements of its distance have been dominated by the Tully-Fischer relation; the Cosmicflows-3 data give a distance modulus of $(m - M)_0 = 31.422 \pm 0.071$ based on the method (Tully et al., 2016). However, Sabbi et al. (2018) recently measured it in a survey using the TRGB. They obtained distances using three distinct fields in the galaxy and obtained different distance moduli for each. Their values of $(m-M)_0 = 30.33\pm0.4, 30.38\pm0.54$, and 30.28 ± 0.33 are consistent, but have relatively large errors and demonstrate the difficulties associated with TRGB measurements.

210 PNe were identified in the MUSE data, with 141 of those constituting the complete sample brighter than 28.3 mag. There are no radial velocity dispersion measurements for NGC 1512 in the literature. However, it is reasonable to expect the dispersion to be small since the galaxy is a face-on spiral. An estimate can be made from the observation that the velocity dispersion perpendicular to the disk in the solar neighborhood is ~ 20 km/s. Given that the MUSE observations are closer to the center than the sun is to the center of the Milky Way, I expect the value to be slightly higher and adopt the loose estimate of 50 km/s. Although this estimate is rough, it should not make much difference since the assumed 100 km/s velocity resolution requires at least a 2σ velocity separation if the actual σ_v is 50 km/s or less. That means that it is likely that $< 5\%$ of spatial blends would be spectroscopically separable in NGC 1512. I took the reddening to be E(B-V) = 0.0091 and obtained $(m - M)_0 = 31.428^{+0.045}_{-0.076}$ (19.3 Mpc) using the new formulation of the PNLF. The classic fit (without blends) gave $(m - M)_0 = 31.36^{+0.04}_{-0.06}$ (18.7 Mpc). Allowing blends once again extended the distance (as expected), but this time only marginally, as seen in Figure 4.4. This is an important result for the new PNLF because it demonstrates that when the galaxy does not have any obviously overluminous sources, the blended fit does not deviate strongly from the classic fit.

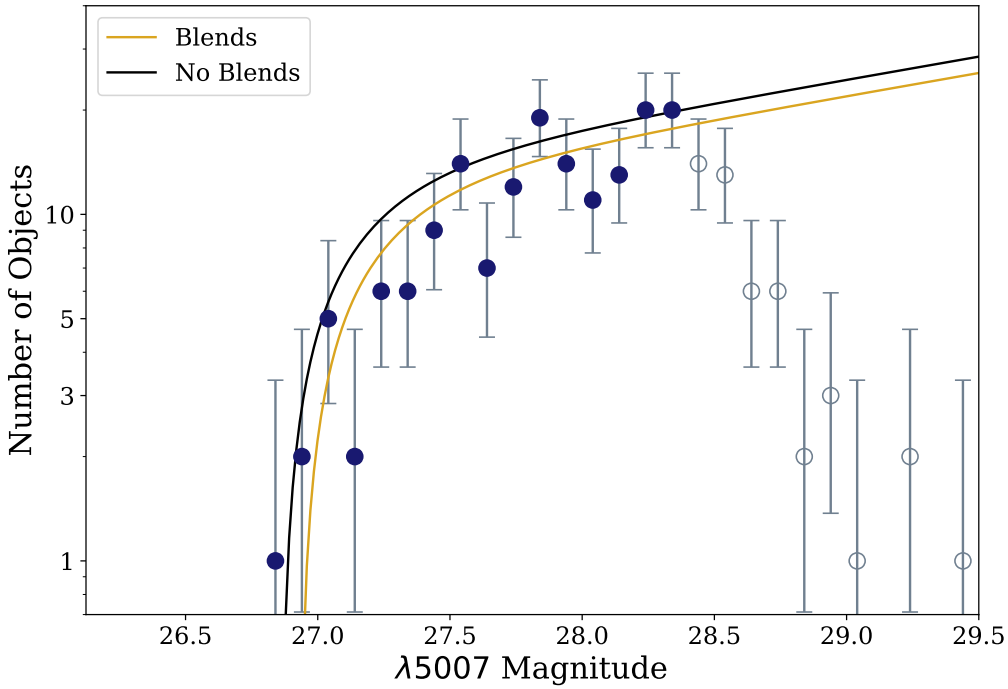

Figure 4.4: The observed PNLF for NGC 1512 (0.1 mag bins) and the fits with and without blends. Notice that the blended fit has not generated a distance too different from the no-blend fit.

Given the extent to which the fitting algorithm has to be changed to incorporate blends (see Section 3.3), this is far from a trivial result.

Galaxy	Blended PNLF Distance	Classic PNLF distance	$\Delta\mu$(Blends - Classic)
Antennae	$31.84^{+0.05}_{-0.06}$	$31.75^{+0.03}_{-0.05}$	0.09
NGC 1399	$31.38^{+0.04}_{-0.03}$	$31.19^{+0.04}_{-0.05}$	0.51
NGC 1351	$31.40^{+0.06}_{-0.13}$	$31.25^{+0.05}_{-0.7}$	0.15
NGC 1512	$31.428^{+0.045}_{-0.076}$	$31.36^{+0.04}_{-0.06}$	0.068

Table 4.1: The distance results for the 4 test galaxies used in this thesis. The distances are given as distance moduli, and the final column gives the difference between the distance moduli calculated using the blended model and that calculated without allowing for blends.

4.6 Discussion

The results for the 4 test galaxies given here (and shown in Table 4.1) are very exciting. Only the Fornax galaxies had previous PNLF distances, and the value I found without incorporating blends agreed excellently with the NGC 1399 distance and somewhat well with the NGC 1351 value found using the same data. This should hardly be surprising, but it lends validity to the other distances I found using the PNLF without blends, both of which were shorter than the recent distances found to the galaxies using other, generally reliable methods, clearly recreating the problem which has led to the downfall of the PNLF. Meanwhile, the fits including blends not only extended the distances, but extended them into good agreement with the other methods in all cases except NGC 1399. Incorporating blends should obviously lead to larger implied distances, since the new foot on the PNLF allows for brighter objects, but it is hard to predict just how much larger the new distances will be when each object is fitted with its own PNLF. It is extremely reassuring to see that blending is capable of *completely* accounting for the offset observed in the PNLF at around 20 Mpc. In fact, the blended distances seem to be very slightly greater than the comparison distances for the 2 late-type galaxies. Given that all the errors quoted are purely statistical and much more work needs to be done to fully specify the uncertainty in the blended fits, it is too early to tell whether blends are over-correcting for the PNLF's past shortfalls. In fact, such an effect would be hard to argue, even if there were no additional errors inherent to the method, because the scatter in

measurements to all the galaxies tested here is well more than the difference between the blended PNLF distance and the other values.

Another exciting feature of these results is the consistency regardless of galaxy type. I tested the new method on two early- and two late-type galaxies, and the improvement over the standard PNLF results was similarly good in both cases. However, the late-type galaxies I tested did see smaller increases in their distances compared to the ellipticals when comparing the blended and classic PNLF fits. This could point to a variation in the extent of the PNLF offset based on galaxy type, but 4 test galaxies is not enough to establish such a difference.

There are still some questions to be raised with these results. Firstly, while the blended distance results are impressive, the distance to the Antennae is arguably not very consistent with the SNIa and TRGB measurements to the galaxies. In fact, this was the only case where the classic PNLF distance was actually greater than the comparison results. This points to the possibility of a zero-point error in the MUSE data for the Antennae. This is entirely possible, since the data were not taken with the PNLF in mind. Alternatively, given the unique nature of the galaxy, these results could point to potential issues in the distances computed with other methods. After all, this is where the PNLF can shine: as a double check on distances computed with methods like SNIa capable of probing much deeper into the Hubble Flow. The other questionable result is the blended distance for NGC 1399. While the classic distance showed excellent agreement with the previous PNLF distance, the new blended fit is still somewhat short of other methods. A distance comparable to SBF measurements would require a large amount of blends to be present in this data. It would not be altogether surprising if there were a surplus of blends in NGC 1399; the galaxy is very bright, likely very thick, and in the middle of a very massive cluster. These are just the sort of conditions which demanded a serious consideration of blends. On the other hand, it has a large velocity dispersion which means many spatial blends should be spectroscopically separable. I would argue the issue is most likely another artifact of the sub-par data and a reflection of the difficulty of plotting the blended model. The way the PNLF histogram for NGC 1399 appears in Figure 4.2 does suggest that there were different viewing conditions between the pointings used for

the galaxy. The solid improvement in the distance to NGC 1399 compared to the standard PNLF, despite the clearly strange data, is a testament to how successful this first trial of the blended PNLF has been.

Chapter 5

Conclusions

In this thesis, I have explored the past success and issues with the PNLF as a distance indicator, presented a new formulation for modeling galactic PNLFs which incorporates the possibility of line-of-sight PNe superpositions, and tested my new formulation on a diverse sample of 4 galaxies. Using simulations, I demonstrated that blending is a viable source of the overluminous objects observed in past PNLF studies and verified that the new, convolved model for the PNLF is capable of accurately accounting for the effects of contamination by blended PNe. The results I obtained using the new PNLF model on archival MUSE data were overwhelmingly positive, in that they extended the distances computed using the classic form of the PNLF into good agreement with reliable methods to each respective test galaxy (except in the questionable case of NGC 1399). I can, therefore, unequivocally conclude that PNe blends as a result of line-of-sight superposition do generate a systematic error in the standard PNLF. In fact, my results indicate that such blends are enough to completely explain the known systematic issues with the PNLF at large distances. Further, given that the blended PNLF was so successful with these test galaxies, which all fall around 20 Mpc away, and that object superpositions become increasingly important at larger distances, this thesis indicates that this new formulation of the PNLF could very likely be the key to extending the method to the desired distances of 40 Mpc or more. It also allows for the exploration of possible unknown systematic errors related to things like dependence of the bright-end cutoff on characteristics of the stellar population. While such a dependence has yet to be observed (except in very low-metallicity galaxies), the blended PNLF could allow for even smaller constraints on the size of such possible systematics. This is extremely important in the chase for a 2% or smaller determination of H_0 with the PNLF.

These results demonstrate the need for high quality, dedicated data from the likes of MUSE in order to hammer down possible systematics and generally constrain errors. There are several key things that dedicated data would ideally include to make the method more robust. Firstly, it would include a bright foreground star for determining the aperture correction. Also, the instrument would conduct standard star measurements as close in time to the science observations as possible in order to help constrain the conversion from MUSE detector counts into standard flux units.

Ideally, the galaxy would be well-sampled, both in the core and in the halo, and observations would be made to understand the galactic characteristics such as velocity dispersion, surface brightness profile, etc.

Despite their promise, the results given here are not entirely final. The distances I presented in Chapter 4 were determined solely by my implementation of the new PNLF methodology and still require extensive testing and cross-checking to ensure they are robust. Future work will include generating test galaxies with embedded PNe and measuring the "distance" using the new method. Such testing will not only ensure robustness within the method, but will also help tune parameters in my implementation (necessary grid densities, etc.) to adequately sample the parameter space. Once this new method is on solid footing, it can be applied to more and more galaxies, especially those from past PNLF studies with known overluminous objects. It will be further important to test the updated PNLF on galaxies farther than 30 or even 40 Mpc, especially those with SNIa measurements. If consistency is achieved at large distances, the PNLF could serve as a new, independent validation for SNIa distances and a new calibration for the method. No other reliable method is currently capable of validating SNIa measurements in the Hubble Flow. The PNLF can not only achieve this, but can expand the number of galactic targets past 20 Mpc because it is effective in early and late type galaxies and does not rely on rare, one-off events. This would make the PNLF a major player in unravelling the Hubble Tension.

There is the additional caveat necessary in every PNLF study: more work is necessary into the stellar evolution behind PNe formation in order to nail down the theory underpinning the PNLF. Until it is understood why the bright-end PNLF cutoff is such an effective distance indicator, the astronomical community can hardly be expected to not look suspiciously upon every result the PNLF produces. In the mean time, however, the mounting empirical evidence in favor of the PNLF should at least be enough to bring it further into the spotlight because it evidently has a lot to teach us.

The results of this thesis point to at least one thing: the future of the PNLF is bright. Although a substantial amount more work is necessary, this thesis clearly demonstrates that the PNLF is ripe

for a revival and has the potential to be among the most important distance indicators in astronomy.

Bibliography

Aniyan, S., Freeman, K. C., Arnaboldi, M., et al. 2018, Monthly Notices of the Royal Astronomical Society, 476, 1909, doi: 10.1093/mnras/sty310

Bacon, R., Accardo, M., Adjali, L., et al. 2010, in Society of Photo-Optical Instrumentation Engineers (SPIE) Conference Series, Vol. 7735, Ground-based and Airborne Instrumentation for Astronomy III, ed. I. S. McLean, S. K. Ramsay, & H. Takami, 773508, doi: 10.1117/12.856027

Badenes, C., Maoz, D., & Ciardullo, R. 2015, The Astrophysical Journal, 804, L25, doi: 10.1088/2041-8205/804/1/L25

Beaton, R. L., Freedman, W. L., Madore, B. F., et al. 2016, The Astrophysical Journal, 832, 210, doi: 10.3847/0004-637X/832/2/210

Bhattacharya, S., Arnaboldi, M., Hartke, J., et al. 2019, Astronomy & Astrophysics, 624, A132, doi: 10.1051/0004-6361/201834579

Blakeslee, J. P., Jordán, A., Mei, S., et al. 2009, The Astrophysical Journal, 694, 556, doi: 10.1088/0004-637X/694/1/556

Bracewell, R. 1999, The Fourier Transform & Its Applications, 3rd edn. (Boston: McGraw-Hill Science/Engineering/Math)

Cardelli, J. A., Clayton, G. C., & Mathis, J. S. 1989, The Astrophysical Journal, 345, 245, doi: 10.1086/167900

Chornay, N., & Walton, N. A. 2021, Astronomy & Astrophysics, 656, A110, doi: 10.1051/0004-6361/202142008

Ciardullo, R. 2006, in Planetary Nebulae in our Galaxy and Beyond, ed. M. J. Barlow & R. H. Méndez, Vol. 234, 325–332, doi: 10.1017/S1743921306003164

Ciardullo, R. 2012, Astrophysics and Space Science, 341, 151, doi: 10.1007/s10509-012-1061-2

Ciardullo, R. 2013, in Advancing the Physics of Cosmic Distances, ed. R. de Grijs, Vol. 289, 247–254, doi: 10.1017/S1743921312021503

Ciardullo, R., Durrell, P. R., Laychak, M. B., et al. 2004, The Astrophysical Journal, 614, 167, doi: 10.1086/423414

Ciardullo, R., Feldmeier, J. J., Jacoby, G. H., et al. 2002a, The Astrophysical Journal, 577, 31, doi: 10.1086/342180

Ciardullo, R., Feldmeier, J. J., Krelove, K., Jacoby, G. H., & Gronwall, C. 2002b, The Astrophysical Journal, 566, 784, doi: 10.1086/338230

Ciardullo, R., & Jacoby, G. H. 1992, The Astrophysical Journal, 388, 268, doi: 10.1086/171150

Ciardullo, R., Jacoby, G. H., Ford, H. C., & Neill, J. D. 1989, The Astrophysical Journal, 339, 53, doi: 10.1086/167275

Coccato, L., Gerhard, O., Arnaboldi, M., et al. 2009, Monthly Notices of the Royal Astronomical Society, 394, 1249, doi: 10.1111/j.1365-2966.2009.14417.x

Davis, B. D., Ciardullo, R., Feldmeier, J. J., & Jacoby, G. H. 2018a, Research Notes of the American Astronomical Society, 2, 32, doi: 10.3847/2515-5172/aab045

Davis, B. D., Ciardullo, R., Jacoby, G. H., Feldmeier, J. J., & Indahl, B. L. 2018b, The Astrophysical Journal, 863, 189, doi: 10.3847/1538-4357/aad3c4

de Vaucouleurs, G., de Vaucouleurs, A., Corwin, Jr., H. G., et al. 1991, Third Reference Catalogue of Bright Galaxies. https://ui.adsabs.harvard.edu/abs/1991rc3..book....D

Dopita, M. A., Jacoby, G. H., & Vassiliadis, E. 1992, The Astrophysical Journal, 389, 27, doi: 10.1086/171186

Feldmeier, J. J., Ciardullo, R., & Jacoby, G. H. 1997, The Astrophysical Journal, 479, 231, doi: 10.1086/512787

Ferrarese, L., Mould, J. R., Stetson, P. B., et al. 2007, The Astrophysical Journal, 654, 186, doi: 10.1086/506612

Ferrarese, L., Mould, J. R., Robert C. Kennicutt, J., et al. 2000, The Astrophysical Journal, 529, 745, doi: 10.1086/308309

Freedman, W. L. 2021, The Astrophysical Journal, 919, 16, doi: 10.3847/1538-4357/ac0e95

Freedman, W. L., Madore, B. F., Gibson, B. K., et al. 2001, The Astrophysical Journal, 553, 47, doi: 10.1086/320638

Galán-de Anta, P. M., Sarzi, M., Spriggs, T. W., et al. 2021, Astronomy and Astrophysics, 652, A109, doi: 10.1051/0004-6361/202140834

Gehrels, N. 1986, The Astrophysical Journal, 303, 336, doi: 10.1086/164079

Gerhard, O., Arnaboldi, M., Freeman, K. C., et al. 2005, The Astrophysical Journal, 621, L93, doi: 10.1086/429221

González-Santamaría, I., Manteiga, M., Manchado, A., et al. 2021, Astronomy & Astrophysics, 656, A51, doi: 10.1051/0004-6361/202141916

Hanes, D. A., & Whittaker, D. G. 1987, The Astronomical Journal, 94, 906, doi: 10.1086/114525

Harris, C. R., Millman, K. J., van der Walt, S. J., et al. 2020, Nature, 585, 357, doi: 10.1038/s41586-020-2649-2

Herrmann, K. A., & Ciardullo, R. 2009, The Astrophysical Journal, 703, 894, doi: 10.1088/0004-637X/703/1/894

Herrmann, K. A., Ciardullo, R., Feldmeier, J. J., & Vinciguerra, M. 2008, The Astrophysical Journal, 683, 630, doi: 10.1086/589920

Hui, X., Ford, H. C., Ciardullo, R., & Jacoby, G. H. 1993, The Astrophysical Journal, 414, 463, doi: 10.1086/173093

Hunter, J. D. 2007, Computing in Science Engineering, 9, 90, doi: 10.1109/MCSE.2007.55

Jacoby, G. H., Ciardullo, R., & Ford, H. C. 1990a, The Astrophysical Journal, 356, 332, doi: 10.1086/168843

Jacoby, G. H., Ciardullo, R., Ford, H. C., & Booth, J. 1989, The Astrophysical Journal, 344, 704, doi: 10.1086/167835

Jacoby, G. H., Walker, A. R., & Ciardullo, R. 1990b, The Astrophysical Journal, 365, 471, doi: 10.1086/169501

Jang, I. S., & Lee, M. G. 2015, The Astrophysical Journal, 807, 133, doi: 10.1088/0004-637X/807/2/133

Koribalski, B. S., & López-Sánchez, Á. R. 2009, Monthly Notices of the Royal Astronomical Society, 400, 1749, doi: 10.1111/j.1365-2966.2009.15610.x

Kreckel, K., Groves, B., Bigiel, F., et al. 2017, The Astrophysical Journal, 834, 174, doi: 10.3847/1538-4357/834/2/174

Kwitter, K. B., & Henry, R. B. C. 2022, Publications of the Astronomical Society of the Pacific, 134, 022001, doi: 10.1088/1538-3873/ac32b1

Lahén, N., Johansson, P. H., Rantala, A., Naab, T., & Frigo, M. 2018, Monthly Notices of the Royal Astronomical Society, 475, 3934, doi: 10.1093/mnras/sty060-

Lam, S. K., Pitrou, A., & Seibert, S. 2015, in Proceedings of the Second Workshop on the LLVM Compiler Infrastructure in HPC, LLVM '15 (New York, NY, USA: Association for Computing Machinery), 1–6, doi: 10.1145/2833157.2833162

Longobardi, A., Arnaboldi, M., Gerhard, O., et al. 2013, Astronomy & Astrophysics, 558, A42, doi: 10.1051/0004-6361/201321652

Macri, L. M., Stanek, K. Z., Bersier, D., Greenhill, L. J., & Reid, M. J. 2006, The Astrophysical Journal, 652, 1133, doi: 10.1086/508530

McMillan, R., Ciardullo, R., & Jacoby, G. H. 1993, The Astrophysical Journal, 416, 62, doi: 10.1086/173215

Méndez, R. H., Riffeser, A., Kudritzki, R.-P., et al. 2001, The Astrophysical Journal, 563, 135, doi: 10.1086/323794

Planck Collaboration, Aghanim, N., Akrami, Y., et al. 2020, Astronomy and Astrophysics, 641, A6, doi: 10.1051/0004-6361/201833910

Pulsoni, C., Gerhard, O., Arnaboldi, M., et al. 2018, Astronomy and Astrophysics, 618, A94, doi: 10.1051/0004-6361/201732473

Reid, W. A., & Parker, Q. A. 2010, Monthly Notices of the Royal Astronomical Society, 405, 1349, doi: 10.1111/j.1365-2966.2010.16635.x

Riess, A. G., Casertano, S., Yuan, W., et al. 2021, The Astrophysical Journal, 908, L6, doi: 10.3847/2041-8213/abdbaf

Riess, A. G., Macri, L., Casertano, S., et al. 2011, The Astrophysical Journal, 730, 119, doi: 10.1088/0004-637X/730/2/119

Riess, A. G., Macri, L. M., Hoffmann, S. L., et al. 2016, The Astrophysical Journal, 826, 56, doi: 10.3847/0004-637X/826/1/56

Roth, M. M., Jacoby, G. H., Ciardullo, R., et al. 2021, The Astrophysical Journal, 916, 21, doi: 10.3847/1538-4357/ac02ca

Sabbi, E., Calzetti, D., Ubeda, L., et al. 2018, The Astrophysical Journal Supplement Series, 235, 23, doi: 10.3847/1538-4365/aaa8e5

Saglia, R. P., Kronawitter, A., Gerhard, O., & Bender, R. 2000, The Astronomical Journal, 119, 153, doi: 10.1086/301153

Saha, A., Claver, J., & Hoessel, J. G. 2002, The Astronomical Journal, 124, 839, doi: 10.1086/341649

Sambhus, N., Gerhard, O., & Méndez, R. H. 2006, The Astronomical Journal, 131, 837, doi: 10.1086/499074

Scheuermann, F., Kreckel, K., Anand, G. S., et al. 2022, Monthly Notices of the Royal Astronomical Society, 511, 6087, doi: 10.1093/mnras/stac110

Schlafly, E. F., & Finkbeiner, D. P. 2011, The Astrophysical Journal, 737, 103, doi: 10.1088/0004-637X/737/2/103

Schönberner, D., Jacob, R., Sandin, C., & Steffen, M. 2010, Astronomy and Astrophysics, 523, A86, doi: 10.1051/0004-6361/200913427

Spriggs, T. W., Sarzi, M., Anta, P. M. G.-d., et al. 2021, Astronomy & Astrophysics, 653, A167, doi: 10.1051/0004-6361/202141314

Tian, Y., & Ko, C.-M. 2016, Monthly Notices of the Royal Astronomical Society, 462, 1092, doi: 10.1093/mnras/stw1697

Tonry, J. L., Dressler, A., Blakeslee, J. P., et al. 2001, The Astrophysical Journal, 546, 681, doi: 10.1086/318301

Tremonti, C. A., Heckman, T. M., Kauffmann, G., et al. 2004, The Astrophysical Journal, 613, 898, doi: 10.1086/423264

Tully, R. B., Courtois, H. M., & Sorce, J. G. 2016, The Astronomical Journal, 152, 50, doi: 10.3847/0004-6256/152/2/50

Tully, R. B., Rizzi, L., Shaya, E. J., et al. 2009, The Astronomical Journal, 138, 323, doi: 10.1088/0004-6256/138/2/323

Tully, R. B., Courtois, H. M., Dolphin, A. E., et al. 2013, The Astronomical Journal, 146, 86, doi: 10.1088/0004-6256/146/4/86

Vanderbeke, J., Baes, M., Romanowsky, A. J., & Schmidtobreick, L. 2011, Monthly Notices of the Royal Astronomical Society, 412, 2017, doi: 10.1111/j.1365-2966.2010.18036.x

Academic Vitae

Owen Chase

EDUCATION

Pennsylvania State University Expected Graduation: May '22
Schreyer Honors College
B.S. Astronomy & Astrophysics
B.S. Statistics
Minor: Mathematics

AWARDS & ACCOLADES

Astronaut Scholar *Awarded '21*
Homer F. Braddock College of Science Memorial Scholarship *'18-'22*
Academic Excellence Scholarship *'18-'22*
University Park Provost Award Scholarship *'18-'22*
Evan Pugh Scholar Award *'21*
President's Sparks Award *'20*
President's Freshman Award *'19*

RESEARCH INTERESTS

- Cosmology: The formation and evolution of the universe and its largest structures from both an observational and theoretical perspective. This includes cosmological parameters, inflation, numerical simulations, dark energy and matter, modified gravity, and relativity.
- Astrostatistics: The application of statistical methodology and data science methods to process large data sets and unveil insights.
- High Energy Astrophysics: The study of AGN and their outflows, black hole formation/dynamics, and particle astrophysics.

RESEARCH & EXPERIENCE

Rethinking the Planetary Nebula Luminosity Function *June '21 – Present*
Penn State University, Department of Astronomy & Astrophysics
Advisor: Dr. Robin Ciardullo
My honors thesis project focuses on analyzing the function used for fitting in PNLF surveys, which are used to calculate galactic distances. My goal is to better understand the shape of the PNLF and investigate whether a new shape would better fit observed data. An improvement to this function could improve all previously measured PNLF distances and make the technique more viable. I use a variety of tools and techniques in this work including Monte Carlo simulations of planetary nebula overlaps, mathematically rebuilding the PNLF to account for overlaps, archival investigations of PNLF studies, and statistical analyses of alternate functions. Python is my main tool for the programming work. This work will not only constitute my thesis project, but will also result in a first author publication.

Investigating X-Ray Emission of Blazar PKS 2005-489 *Jan '21 – Present*
Penn State University, Department of Astronomy & Astrophysics
Advisor: Dr. Felicia Krauss
Use *NuSTAR* X-Ray data and a variety of additional multiwavelength data for PKS 2005-489, a very bright BL Lac object, to better understand its strange emission behavior. I build, fit, and analyze broadband SEDs using data from many different observatories including *Fermi*/LAT, *Swift*/XRT, UVOT, and others to better understand the

source in both low and high states. Understanding the source's strange behavior could improve our understanding of AGN outflows and their underlying physical processes. I conduct data analysis in S-Lang using the ISIS X-Ray analysis tool. I am currently in the final stages of preparation for a paper documenting the results of this project.

Using MUSE to Extend PNLF into Hubble Flow *July '20 – May '21*
Penn State University, Department of Astronomy & Astrophysics
Advisor: Dr. Robin Ciardullo
Participate in an international research team using photometric and spectroscopic data from the MUSE instrument to calculate galactic distances using the Planetary Nebula Luminosity Function. The goal is to establish an accurate and independent value of local H_o to investigate the Hubble tension. I identify PNe on image frames and perform initial photometry using DS9 and Python. Work is ongoing, although my contribution is now mostly in the form of my thesis work.

Searching for and Analyzing Planetary Nebulae *Fall '19 - June '20*
Penn State University, Department of Astronomy & Astrophysics
Advisors: Dr. Robin Ciardullo and Brian Davis
Searched for extragalactic planetary nebulae using spectroscopic data from the Hobby-Eberly Telescope and photometric data from the Hubble Space Telescope. This work was primarily in Python. Further work pending more HETDEX data.

Pulsar Search Collaboratory *Sep '18 - May '19*
Penn State University, Department of Astronomy & Astrophysics
Analyzed data from the Arecibo and Green Bank Observatories to identify/classify pulsar candidates as part of the Penn State instance of the PSC.

PUBLICATIONS

Roth, M.M., Jacoby, G.H., Ciardullo, R., Davis, B.D., **Chase, O.**, Weilbacher, P.M.
Towards Precision Cosmology With Improved PNLF Distances Using VLT-MUSE I. Methodology and Tests. *The Astrophysical Journal*, 916, 1, id.21, arXiv:2105.01982 (2021)

PRESENTATIONS

Posters

Chase, O., Ciardullo, R., Roth, M.M., Jacoby, G.H., Davis, B.D., Weilbacher, P.M. "Toward an Accurate Measure of the Hubble Constant using Planetary Nebulae with VLT-MUSE" *presented at* the 237th meeting of the American Astronomical Society. January 2021. (Held virtually)

TEACHING & OUTREACH

Learning Assistant in Astronomy *Fall '20 & Spring '21*
Worked with students in the 2 core courses of the Astronomy major. Managed 2 hour long 'office hours' meeting weekly.

Carnegie Science Center Buhl Planetarium Volunteer *Summer '17*
Spent over 100 volunteer hours assisting with planetarium productions and giving scientific presentations to guests over the course of the summer.

SKILLS & OTHER ACTIVITIES

Proficient Programming Languages:

- Python, including the numpy and matplotlib libraries
- R and its use in data scraping, manipulation, and analysis including various machine learning techniques including SVM, decision trees, GMM, etc
- Others: S-Lang, LaTeX, Mathematica, Java

Intro to Astronomy Research Summer Course *Summer '19*

University of California, Berkeley

Instructor: Howard Isaacson

Attended weekly online sessions for 10 weeks. Read and discussed numerous research papers and completed tutorials for unix shell, various relevant Python libraries, querying the Gaia database, exoplanetary data analysis, etc.

Second Floor Standup Executive *Spring '21 - Present*

Current vice president of the main PSU standup comedy club. Previously served as treasurer. I've been with the club for more than 5 semesters to date.

Various Coding Competitions/Workshops *'18/'19*

- DevPSU, HackPSU, CodePSU